Tampere University

Jorge Morte Palacios

CELL-FREE MULTI-USER MASSIVE MIMO UNDER CHANNEL NON-RECIPROCITY

Faculty of Information Technology and Communication Sciences
Master of Science Thesis
July 2019

ABSTRACT

Jorge Morte Palacios: Cell-Free Multi-User Massive MIMO Under Channel Non-Reciprocity
Master of Science Thesis
Tampere University
Master of Science
July 2019

In Cell-Free (CF) Massive multiple-input multiple-output (MIMO), a large number of access points (AP) are geographically distributed over the coverage area, and jointly serve a smaller number of users on the same time/frequency resources.

In this thesis, we study the impact of non-reciprocal channels (NRC) and imperfect channel state information (CSI) on Cell-Free massive MIMO systems performance. As non-reciprocity sources, we consider transceiver frequency response mismatches and mutual-coupling mismatches in uplink and downlink analogue processing chains. We study both single-antenna and multi-antenna AP configurations, and in this last case, we also include non-reciprocal mutual coupling in addition to transceiver frequency responses.

We present a novel non-reciprocal channel model based on experimental results from massive MIMO reciprocity calibration tests. Previous models consider that channel non-reciprocity characteristics are fast-varying like random variables; conversely, we consider a model where non-reciprocity values change substantially slower in time, as demonstrated in experimental results. Besides, we derive closed-form analytical expressions of capacity lower bounds for zero-forcing and conjugate beamforming schemes.

The conclusion is that non-reciprocal channels can be a limiting factor for Cell-Free systems performance; nevertheless, only AP mismatches impact on performance while UE mismatches do not affect performance. Furthermore, only phase non-reciprocity degrades MRT performance, whereas both phase and amplitude non-reciprocity degrade ZF performance. Therefore, calibration requirements may dispense with amplitude compensation when APs use MRT scheme, and prioritise phase over amplitude compensation when APs use ZF scheme. Mutual coupling considerately affects both MRT and ZF precoders, but ZF to a greater extent. Hence, calibration procedures should always try to compensate for mutual coupling non-reciprocity.

Keywords: cell-free, massive, mimo, channel reciprocity, downlink, maximum-ratio processing, zero-forcing precoding, frequency response mismatch, conjugate beamforming

PREFACE

This Master's thesis has been written at the Department of Electronics and Communications Engineering at Tampere University in 2018/2019 and financially supported by Tampere University.

I would like to express my gratitude to my thesis supervisor, Professor Mikko Valkama, for the guidance and advice throughout the thesis and to provide the opportunity of working at the Department of Electronics and Communications Engineering, where I could learn the research methodology of scientific works. I also want to thank Orod Raeesi and Ahmet Gokceoglu for their valuable comments and advice.

Tampereella, 26th July 2019

Jorge Morte Palacios

CONTENTS

LIST OF FIGURES

LIST OF TABLES

LIST OF SYMBOLS AND ABBREVIATIONS

L	Number of APs
M	Number of antennas per AP
β	Large-scale coefficient
τ_u	Pilot samples
τ	Coherence interval
g	Downlink channel
h	Uplink channel
5G	Fith-Generation
ADC	Analogue-to-Digital Converter
AP	Access Point
BS	Base Station
CDF	Cumulative Distribution Function
CF	Cell-Free
CPU	Central Processing Unit
CSI	Channel State Information
DAC	Digital-to-Analogue Converter
DL	Downlink
FDD	Frequency-Division Duplex
GA	Genie Aided
MIMO	Multiple-Input Multiple-Output
MMSE	Minimum Mean Square Error
NRC	Non-Reciprocal Channel
OFDM	Orthogonal Frequency Division Multiplexing
PL	Propagation Losses
RF	Radio Frequency
RMSE	Root Mean Square Error
RX	Receiver
SINR	Signal-to-Interference-and-Noise Ratio
SNR	Signal-to-Noise Ratio

TDD	Time-Division Duplex
TX	Transmitter
UatF	Use-and-then-Forget
UE	User Equipment
UL	Uplink

1 INTRODUCTION

Global demand for wireless connectivity is continuously increasing, both in terms of data peak rates and the number of devices connected to the network. In addition to higher bit rates, users are also expecting more reliable connections than previous mobile generations. Those demands involve a larger bandwidth or additional base stations to achieve the requirements of spectral efficiency.

Massive MIMO technology promises to achieve those requirements without employing a much higher bandwidth. Since system bandwidth cannot increase indefinitely, massive MIMO has arisen as one of the most promising technologies.

This thesis addresses Cell-Free massive MIMO systems, which is one promising technology to reach those requirements. Cell-Free massive MIMO systems combine the deployment of multiple access points and the use of a large number of antennas. Additionally, we analyse the impact of channel non-reciprocity, which is a relevant problem in massive MIMO systems.

1.1 Motivation

Massive MIMO, considered a key enabling technology for 5G systems, consists in an array equipped with a large number of antenna elements M serving K users simultaneously on the same time-frequency resources where $M >> K$ [24, 25].

An essential requirement for using massive MIMO is to have channel state information (CSI) at the base station. For that purpose, systems operate in time division-duplex mode and use the uplink channel estimates as downlink channel estimates [32]. In chapter 2, we describe more extensively massive MIMO functioning and explain the primary considerations to understand massive MIMO technology fully.

Non-reciprocal channels (NRC) consist of channels whose frequency response is not the same in uplink and downlink [9, 22, 40, 41]. Hence, NRC implies a degradation of the CSI if not calibration procedure is carried out [39, 52]. In chapter 3, we present a non-reciprocal channel model and the assumed considerations during this work.

Cell-Free massive MIMO systems exploit a traditional large amount of antenna elements but in a distributed manner [30, 34]. A large number of geographically distributed APs L serve simultaneously over the same time/frequency resources a much smaller number of

users K, in contrast to small-cell systems, where the APs do not cooperate coherently [31]. Chapter 4 details Cell-Free systems, presents analytical derivations for achievable rates and explains Cell-Free systems deployment parameters.

This work aims to research and analyse a performance evaluation and modelling of Cell-Free massive MIMO systems under non-reciprocal channels.

1.2 Contributions

We summarise the novel contributions of this thesis as follows

- In contrast to existing literature, this work considers a Cell-Free system deployment under non-reciprocal channels, we derive closed-form analytical expressions of the output SINR for practical ZF and MRT precoders in the presence of NRC.
- In contrast to existing literature, we present a more physically-inspired NRC model. Previous literature considers that channel non-reciprocity characteristics are fast-varying like random variables [26, 38, 39, 40, 41]; conversely, we consider a model where non-reciprocity values change substantially slower in time, as demonstrated in experimental results [46].
- In contrast to [29, 31], we consider fully distributed single-antenna APs and semi-distributed multi-antenna APs, including both transceiver frequency mismatches and mutual-coupling non-reciprocal responses.

1.3 Thesis outline

This thesis is organised as follows

- Chapter 2 covers the basic theoretical foundations of massive MIMO.
- Chapter 3 presents the problem of hardware impairments and proposes a hardware model that captures non-reciprocity of transceiver frequency responses and mutual coupling.
- Chapter 4 considers a Cell-Free deployment, first presenting the system model and then all derivations of the lower capacity bounds of MRT and ZF precoders. It also includes how cell deployment is carried out, detailing all system parameters.
- Chapter 5 provides discussions based on the numerical results of systems and models presented throughout the work.
- Finally, chapter 6 summarises the results and lists possible future lines of research.

2 MASSIVE MIMO BACKGROUND

2.1 Introduction

In this chapter, we present the minimum theoretical background of Massive MIMO needed to understand the following work. Firstly, we describe multipath propagation environments, including some essential metrics as coherence time and coherence bandwidth, and we present the physical channel model used in this work. Secondly, we briefly explain the OFDM systems insofar as it has implications for MIMO systems, and finally, we survey the most critical Massive MIMO concepts such as capacity bounds, linear processing techniques or duplexing modes.

2.2 Multipath physical channel

An analogue signal is transmitted through a wireless channel between the mth transmission antenna to the kth reception antenna. In practical scenarios, the environment is reflective, i.e. the signal travels through different paths, and the receiver captures signals which have experienced different propagation conditions [44, 51].

The signals propagated in different paths will have different delays, attenuation and phase shifts [37]. This multipath effect can be express in a baseband equivalent given by

$$p_{mk}(t,\tau) = \sum_{n=1}^{N_S} \alpha_n(t) e^{-j\phi_n(t)} \delta(\tau - \tau_n(t)) \tag{2.1}$$

where $\alpha_n(t)$, $\phi_n(t)$, $\tau_n(t)$ are the attenuation, phase shift and delay, respectively. Since the environment is continuously changing, the parameters which define the channel response depend on the time, producing a time-varying channel [37].

Coherence time To measure how fast channel characteristics change over time, the coherence time is defined as the maximum time interval between two highly correlated channel taps [37]. From a practical point of view, the coherence time can be considered as the time interval within which the channel response remains constant.

If the symbol time is greater than the coherence time, we can assume that the propagation signal is subject to stationary channel conditions.

Coherence bandwidth The channel frequency response is defined at a time t as the Fourier transform of h(t, τ) with respect to τ as follows [37]

$$P_{mk}(t,f) = \int_{-\infty}^{\infty} p_{mk}(t,\tau) e^{-j2\pi f\tau} d\tau \tag{2.2}$$

Coherence bandwidth as a metric of channel frequency flatness characterises variations of frequency response relative to frequency. This statistical measure expresses the maximum bandwidth or frequency interval in which two frequencies are likely to experience a highly correlated channel coefficient. Coherence bandwidth in rad/s is typically approximated using [51]

$$W_c \approx \frac{2\pi}{D} \tag{2.3}$$

where D is the multipath delay spread in seconds.

Frequency non-selective and slowly-fading channels In case the coherence time is much greater than the symbol duration the channel is slow faded and the channel response becomes independent of t being written as [37]

$$p_{mk}(\tau) = \sum_{n=1}^{N_S} \alpha_n e^{-j\phi_n} \delta(\tau - \tau_n) \tag{2.4}$$

If the coherence time is larger than the symbol duration T_s, and if the coherence bandwidth is also greater than the bandwidth of the symbol, we can assume that $\tau_n \approx 0$, thus the physical channel response in a certain bandwidth interval can be approximated by

$$p_{mk}(\tau) \approx \rho_{mk} e^{j\phi_{mk}} \delta(\tau) \tag{2.5}$$

where ρ represents the attenuation and ϕ represents the phase shift. The physical channel is commonly modelled as

$$p_{mk} = \sqrt{\beta_{mk}} h_{mk} \tag{2.6}$$

where β_{mk} is the average path loss or large-scale coefficient and h_{mk} models the fast fading response, known as the small-scale coefficient. The small-scale coefficient is modelled as a standard complex normal distribution, i.e. $\mathcal{CN}(0,1)$. This model is widely used for indoor and non-line-of-sight outdoor environments [25, 51].

2.3 OFDM systems overview

Orthogonal frequency-division multiplexing is a method widely used in wideband digital communication applications. The concept behind OFDM is simple; a high rate stream is dividing into N_{sc} parallel streams modulated onto N_{sc} sub-carriers instead of a single wideband stream.

In OFDM, unlike more classical FDM-based approaches, the superposition of sub-carriers with the appropriate frequency separation is allowed by taking advantage of frequency orthogonality [44].

The most crucial advantage of OFDM for this work is frequency selectivity, in case the channel is frequency selective the equalisation techniques in FDM at the receiver require a significant complexity [37, 44]. Contrariwise, in OFDM the total bandwidth is split among many orthogonal sub-bands, and since coherence bandwidth of the system is higher than sub-channel bandwidth, the channel response can be assumed to be flat all over the sub-channel bandwidth. Block-channel fading implies an extremely simple equalisation since each sub-carrier only needs to be weighted by a coefficient which depends on the channel gain and phase.

This OFDM advantage allows us to use the frequency non-selective channel model that we have previously presented.

2.4 Massive MIMO systems

The main limitation of wireless communications is at the physical layer; information theory concepts limit the transmitted amount of information. The demand for wireless throughput is increasing irremediably, and yet the available spectrum is increasing any more. This limitation poses a difficult challenge, how to increase system capacity continuously if we cannot increase bandwidth endlessly. The proposals focus on three possibilities [24]: 1) Operating in the unused spectrum; 2) Increasing the access point density; 3) Increasing the number of antennas at access points or user terminals. MIMO systems are shown to be the best option to improve spectral efficiency.

Multi-user Massive MIMO consists of a base station serving to a relatively large number of users in the same time-frequency resources. The K user equipment are assumed to have a single antenna, and the base station side is assumed to be equipped with M antennas, where M is much larger than K [8, 24, 25].

In time-division duplex operation (TDD), the access points acquire the CSI by uplink pilots sent simultaneously from all the users, and using the reciprocity between the uplink and downlink channels perform the beamforming [25]. To be able to rely on channel reciprocity, a calibration process has to be performed on the transceiver hardware [46]. In the following chapters, we present a baseband model of non-reciprocal channels and their impact on the performance of multi-user massive MIMO.

Increasing the number of antennas always improves the achievable rate, reduces the total radiated power or increases the number of users that can be served in the same time-frequency resources [8]. This increment also simplifies the signal processing due to the channel hardening, i.e. the small-scale fading h_{mk} cancels out and frequency dependence disappears when M tends to infinity [25]. By virtue of the law of large numbers,

the effective channel gain $||\mathbf{g}_k||^2$ is close to its expected value $\mathrm{E}\{||\mathbf{g}_k||^2\}$, that implies that the users do not need to estimate the instantaneous effective channel gain to obtain a similar achievable rate [8, 25]. Later in this thesis, we survey how cell-free and centralised Massive MIMO systems behave in terms of channel hardening, extracting some conclusions about what capacity bounds should be used to characterise the channel capacity rigorously.

2.4.1 Time-division vs frequency-division duplexing

Multi-user massive MIMO systems require CSI in the transmitter and, depending on the specific scenario, also in the receiver, e.g. if the user terminal is equipped with more than one antenna, it is possible to send more than one data stream to the same user or apply diversity techniques to reduce the probability of fading [25]. Channel information should be obtained either by estimating the uplink channels with pilot signals or by feedback from the receiver to the transmitter.

In time division duplex (TDD) operation, the access point side learns channel information from uplink pilots sent by users. Since the physical channel is reciprocal because the response between two antennas is the same regardless of direction due to the reciprocity theorem, APs use the uplink channel estimate as downlink channel estimate. For that reason, TDD operation is the most common scheme used in massive MIMO [8, 25].

In frequency division duplex (FDD) operation, the user equipment learns the downlink channel from pilots transmitted from the access point side and sends it back to the access points. Therefore, the overload depends on the number of antennas on the access point side, which can be problematic in high mobility or high-frequency scenarios, where the coherence interval is minimal. The signalling overhead scales linearly with both the number of antennas at the access points and with the user equipment, that is why FDD massive MIMO can only be supported in specific low-mobility and low-frequency scenarios.

Although TDD is the most common duplexing mode, it has some disadvantages comparing with FDD. We are transmitting over the entire bandwidth half the time, so the average radiated power is 3 dB lower than in FDD. Therefore, the SINR is also 3 dB lower. Since everyone in the cell has to operate uplink or downlink at the same time and the distances between users and base stations can be vast, a guard period is needed to prevent interference between uplink and downlink [8].

2.4.2 Spatial diversity and spatial multiplexing

The existence of multiple antennas also means the existence of different propagation paths. To take advantage of these multiple paths, we can send redundant information

along the multiple paths or independent data streams [25].

- **Spatial diversity:** Send or receive redundant data streams through multiple spatial paths to improve the reliability and range.
- **Spatial multiplexing:** Send independent data streams through multiple spatial paths to improve the data rate of the system.

In spatial diversity techniques, the same data is sent along the multiple propagation channels, and if the multiple channels are independent, the fading can be combated because the fading suffered by each data stream is different. This redundancy implies that the probability of a data stream suffering less fading is higher than with only one channel [8].

2.4.3 Capacity bounds preliminaries

Since each user equipment is assumed to be equipped with one antenna, the resulting effective channel from the base station antennas to the user is a scalar point-to-point channel [25, 33]. That means that when a single input data symbol is transmitted, the user receives a single output data symbol.

Let us express the channel model as follows [33]

$$y_k = c_k s_k + \sum_{k' \neq k}^{K} c_{k'} s_{k'} + n_k \tag{2.7}$$

where c_k is the scalar point-to-point channel of the k-th user, s_k is the symbol intended for the k-th user and n_k is additive noise.

Let $I(\cdot,\cdot)$ be the mutual information between the channel input s_k and the output y_k when the receiver knows the side information g [25, 36, 48]. The capacity of a general point-to-point scalar channel assuming Gaussian distribution of the transmitted symbols, $s_k \sim \mathcal{CN}(0,1)$, is then given by [33]

$$C_k = I(s_k; y_k, g) = h(s_k) - h(s_k|y_k, g) \tag{2.8}$$

Applying the property that entropy is invariant to translation and the fact that conditioning reduces the entropy [25], we have

$$C_k \geq \log_2(\pi e) - h(s_k - \alpha y_k|g) = \log_2(\pi e) - \mathbb{E}\{\log_2(\pi e \mathbb{E}\{|s_k - \alpha y_k|^2|g\})\} \tag{2.9}$$

The term $\mathbb{E}\{|s_k - \alpha y_k|^2|g\}$ depends on the side information known at the receiver, we address two cases; when the user has no channel information, i.e. $g = \emptyset$, and when the user knows the effective channel, i.e. $g = c_k$. Therefore and computing α as the LMMSE

estimate of s_k [19]

$$\mathbb{E}\{|s_k - \alpha y_k|^2 | g\} = 1 - \frac{|\mathbb{E}\{c_k|g\}|^2}{\sum_{k'=1}^{K} \mathbb{E}\{|c_{k'}|^2|g\} + 1} \tag{2.10}$$

Then, we have

$$C_k \geq \mathbb{E}\left\{\log_2\left(1 + \frac{|\mathbb{E}\{c_{k'}|g\}|^2}{\sum_{k'=1}^{K} \mathbb{E}\{|c_k|^2|g\} - |\mathbb{E}\{c_k|g\}|^2 + 1}\right)\right\} \tag{2.11}$$

In the case of no side information at the receiver, the capacity bound is called Use-and-then-Forget and the receiver uses the channel statistics to detect the received symbol, yielding

$$C_k \geq \log_2\left(1 + \frac{|\mathbb{E}\{c_k\}|^2}{\sum_{k'=1}^{K} \mathbb{E}\{|c_{k'}|^2\} - |\mathbb{E}\{c_k\}|^2 + 1}\right) \tag{2.12}$$

Conversely, if the receiver knows the effective downlink channel, the capacity bound is then called Genie-Aided and reads

$$C_k \geq \mathbb{E}\left\{\log_2\left(1 + \frac{|c_k|^2}{\sum_{k' \neq k}^{K} |c_{k'}|^2 + 1}\right)\right\} \tag{2.13}$$

We apply Jensen's inequality, which has been shown to provide tight rates in massive MIMO problems, then the capacity yields [25]

$$C_k \geq \log_2\left(1 + \frac{\mathbb{E}\{|c_k|^2\}}{\sum_{k' \neq k}^{K} \mathbb{E}\{|c_{k'}|^2\} + 1}\right) \tag{2.14}$$

The effective number of bits captured in a symbol is measured in bits per channel use (bpcu), when the transmitted symbol is contained in a time-frequency resource with a certain bandwidth and symbol time, the rate is expressed as spectral efficiency and measured in bits per second per Hertz (bps/Hz) [25].

2.4.4 Linear processing

To obtain optimal performance and benefit from the use of multiple antennas, AP should use complex signal processing techniques. Since complexity increases exponentially with the number of antennas, base stations can use linear processing schemes which are shown to be nearly optimal when the number of antennas at the base station is enormous [33].

Throughout this work, we focus on analysing downlink performance. Therefore, we only study linear precoding techniques, where the signal transmitted from M antennas is a linear combination of the symbols intended for K users.

We review two classic linear multi-user precoders

Maximum-Ratio transmitter or Conjugate beamforming By using MRT, the base station aims to maximise the signal-to-noise ratio of each user disregarding the interference produced by other users [55].

The main advantage is that the required signal processing is straightforward, since only one matrix multiplication is needed, and this also implies that the MRT can be implemented in a distributed manner.

The $M \times K$ MRT precoding matrix is given by [8, 25]

$$\mathbf{W} = \mathbf{H}^{\dagger} \tag{2.15}$$

where $\mathbf{H}$ is the channel matrix.

Zero-Forcing precoder In contrast to MRT, Zero-Forcing precoder aims to minimise the inter-user interference without taking into account the effect of noise. With ZF, the multi-user interference is entirely avoided by projecting each stream onto an orthogonal component [55].

The $M \times K$ ZF precoding matrix is given by [8, 25]

$$\mathbf{W} = \mathbf{H}^{\dagger}(\mathbf{H}\mathbf{H}^{\dagger})^{-1} \tag{2.16}$$

where $\mathbf{H}$ is the channel matrix.

ZF precoder satisfies the orthogonal condition in this manner

$$\begin{cases} \mathbf{w}_k^T \mathbf{h}_k \neq 0 \\ \mathbf{w}_{k'}^T \mathbf{h}_k = 0 \quad \forall k' \neq k \end{cases}$$

ZF precoder has several advantages, e.g. the signal processing is simple (not as simple as MRT due to pseudo-inverse computation) and works well under interference conditions. In an ideal scenario, we could increase the SINR as much we desired by increasing the transmitted power. Conversely, ZF performs poorly with a small number of users and under noise-limited scenarios.

2.4.5 Performance metrics

In this work, we use the following metrics to evaluate the performance of different systems under certain conditions.

Achievable rate We use the derived capacity lower bounds in the previous section to obtain the per-user spectral efficiency, and we add the overhead penalty. As we commented, when the system operates in TDD, part of the coherence interval is used for

training purposes. Therefore it is necessary to take pilot overhead into account by weighting the obtained capacity with [8]

$$F_{oh} = 1 - \frac{\tau_u}{\tau} \tag{2.17}$$

where τ_u is the pilot length in samples and τ is the coherence interval duration in samples.

Cumulative distribution function When we simulate and replicate the deployment of a cell either in a distributed or centralised way, we use the cumulative distribution function of the per-user spectral efficiency. By doing so, we obtain the 5th and 95th percentiles, which give information about the minimum per-user spectral efficiency that the 95 and 5 per cent of the users experience, respectively.

The cumulative distribution function of a random variable is defined as [13, 45]

$$F_x(x) = P(X \leq x) \tag{2.18}$$

Notwithstanding, we obtain the CDF from numerical results, i.e. we choose an adequate number of cell realisations, then we simulate the system obtaining a relevant set and, thereupon, we estimate the CDF.

3 IMPERFECT HARDWARE MODELLING

Channel reciprocity has been considered one of the main advantages of TDD over FDD systems [32]. Since the uplink and downlink transmissions share the same frequency band, the transmitter can use the uplink channel estimates to perform precoding techniques in the downlink transmission. TDD beamforming techniques are theoretically possible when the uplink and downlink transmissions occur in the same coherence interval, but in practical systems, the reciprocity might not be perfect within the same coherence interval.

In FDD systems, the downlink channel is estimated at the user equipment and sent back to the base station. Thereupon, the pilot training entails a substantial overhead when the number of antennas is large. Manifold works try to overcome training overhead [2, 3]; nevertheless, it remains a significant challenge. Hence, to be able to take advantage of the benefits of massive MIMO, the system needs to operate in TDD mode and consider that the uplink and downlink channels are the same within a coherence interval.

A classical Massive MIMO system consists of a baseband processing section and multiple RF front-ends connecting the baseband section to each antenna [47]. In general, the baseband section is all-digital, and the RF front-end is analogue, a DAC/ADC connects both sections in TX or RX cases, respectively [28].

The TX signal is modulated at the baseband section and then is up-converted and amplified in the analogue front-end. Similarly, the RX signal is first amplified and down-converted by the analogue front-end and then demodulated in the baseband section.

In this chapter, we introduce a model that captures the transceiver frequency responses of both transmit and receive analogue circuitry, and also a model of mutual coupling and its non-reciprocity.

3.1 Analogue circuitry impairments

A considerable problem appears in massive MIMO when we cannot assume the system reciprocity because the frequency behaviour of the analogue transmitter and receiver front-ends are not symmetric.

The analogue hardware components, in both, transmit and receive analogue processing chains, are different. That difference entails that we cannot rely on channel reci-

procity without performing a calibration process, and errors in the calibration of hardware in downlink and uplink might degrade the achievable rate and spectral efficiency.

Since the TX and RX analogue front-ends are physically different, the overall response is also different. The exact modelling and simulation of the RF front-end response are considerately complicated and time-consuming. Therefore, a baseband equivalent model for the impairments is usually used, instead of modelling the behaviour of the RF front-end, we characterise how these imperfections affect the baseband signal.

The discrete signal to be transmitted is filtered by a band-limiting filter and then transmitted through the physical multipath channel. The transmission filter includes the frequency response of the DAC and all the RF circuits, e.g. mixers, filters and power amplifiers.

All the analogue processing chain in both transmission and reception is treated as a block response, i.e. the frequency response is considered to be flat all over the bandwidth of the sub-carrier. For the sake of simplicity and without loss of generality, the following model applies to a single frequency tap, but it can be easily generalised to the rest of the frequency taps.

We compact the analogue circuitry responses in a model presented in [1, 26] given by

$$r(t, P, T) = A(t, P, T)e^{j\phi(t,P,T)} \tag{3.1}$$

where A represents the amplitude response and ϕ represents the phase response. The RF response is a function of different environmental factors, i.e. time t, power P and temperature T.

Taking a reference, the model can be expressed as [1]

$$A_x(t_1, P_1, T_1) = A_x(t_0, P_0, T_0) + a_x\Delta t + b_x\Delta P + c_x\Delta T \tag{3.2}$$

$$\phi_x(t_1, P_1, T_1) = \phi_x(t_0, P_0, T_0) + a'_x\Delta t + b'_x\Delta P + c'_x\Delta T \tag{3.3}$$

where a_x, b_x, c_x, a'_x, b'_x, c'_x denote the linear coefficients which model the variations with respect to the environmental factors, these values are obtained measuring transceivers in practical conditions.

Let us define the transceiver frequency response diagonal matrices at the receiver and transmitter of the access points and users as $\mathbf{R}$, $\mathbf{T}$, $\mathbf{B}$, $\mathbf{A}$, respectively.

Next, the frequency response reciprocity errors can be captured in a reciprocity error matrix given by

$$\mathbf{E}_a = \mathbf{T}\mathbf{R}^{-1} \tag{3.4}$$

$$\mathbf{E}_u = \mathbf{B}\mathbf{A}^{-1} \tag{3.5}$$

where $\mathbf{E}_a$ and $\mathbf{E}_u$ represent the differences between the downlink and uplink channels at the access points and the users, respectively.

The effective channel in uplink and downlink capture the reciprocal physical channel and the RF circuitry responses at the transmitter and receiver, respectively, as

$$\mathbf{H} = \mathbf{RPA} \tag{3.6}$$

$$\mathbf{G} = \mathbf{BP}^{\mathsf{T}}\mathbf{T} \tag{3.7}$$

Based on the error matrices, the relation between the uplink and downlink channels is given by

$$\mathbf{G} = \mathbf{E}_u\mathbf{H}\mathbf{E}_a \tag{3.8}$$

Previous works study how stable are those RF circuitry mismatch responses over time, and they survey how often the calibration process should be performed to restore the channel reciprocity [46]. They perform experimental evaluations of the stability of reciprocity calibrations, concluding that calibration can be performed very infrequently, i.e. tens of minutes. From these results, the reciprocity matrices can be treated as unknown constants of the form

$$r_x = A_x e^{j\phi_x} \tag{3.9}$$

Generalising the proposed model, each frequency tap has each own physical channel and RF circuitry responses $\mathbf{A}[l]$, $\mathbf{B}[l]$, $\mathbf{T}[l]$, $\mathbf{R}[l]$, $\mathbf{P}[l]$ where l denotes the frequency tap. The frequency response of RF circuitry is usually smooth over a certain bandwidth, and the calibration process can take advantage of the correlation between frequency responses to increase the estimation accuracy.

In practice, the separate modelling of $\mathbf{R}$, $\mathbf{T}$, $\mathbf{B}$, $\mathbf{A}$ is more accurate than directly the compound error $\mathbf{E}_a$ and $\mathbf{E}_u$ [26].

The independent random variables A_x and ϕ_x model the randomness of the RF circuitry, the amplitude and phase responses are assumed to have an expected value of μ_A and μ_ϕ and a variance of σ_A^2 and σ_ϕ^2, respectively.

To model the reciprocity level at the front-ends, we define the covariance between the parameters of the uplink and downlink transceiver frequency responses as

$$\mathsf{Cov}(A_{ur,k}, A_{ut,k}) = \nu_{A_{\mathsf{UE}}}\sigma_A^2 \tag{3.10}$$

$$\mathsf{Cov}(A_{ar,m}, A_{at,m}) = \nu_{A_{\mathsf{AP}}}\sigma_A^2 \tag{3.11}$$

$$\mathsf{Cov}(\phi_{ur,k}, \phi_{ut,k}) = \nu_{\theta_{\mathsf{UE}}}\sigma_\theta^2 \tag{3.12}$$

$$\mathsf{Cov}(\phi_{ar,m}, \phi_{at,m}) = \nu_{\theta_{\mathsf{AP}}}\sigma_\theta^2 \tag{3.13}$$

where ν denotes the reciprocity level, when $\nu = 1$ the responses in uplink is downlink are the same, i.e. the channel is reciprocal.

Note that we model the uplink and downlink frequency responses separately to compare reciprocal and non-reciprocal channels under the same conditions. If we only modelled the difference between uplink and downlink, the frequency responses would not vary in a

reciprocal case at each realisation, and this would not be a fair comparison.

Next, we present a metric for the non-reciprocity level of the frequency responses of the analogue front-ends known as mean squared error (MSE) given by

$$\varepsilon^2_{A_{\mathsf{UE}}} = \mathsf{E}\{|A^{\mathsf{d}}_{F_k} - A^{\mathsf{u}}_{F_k}|^2\} = (1 - \nu_{A_{\mathsf{UE}}})\sigma^2_A \tag{3.14}$$

$$\varepsilon^2_{A_{\mathsf{AP}}} = \mathsf{E}\{|A^{\mathsf{d}}_{B_m} - A^{\mathsf{u}}_{B_m}|^2\} = (1 - \nu_{A_{\mathsf{AP}}})\sigma^2_A \tag{3.15}$$

$$\varepsilon^2_{\theta_{\mathsf{UE}}} = \mathsf{E}\{|\theta^{\mathsf{d}}_{F_k} - \theta^{\mathsf{u}}_{F_k}|^2\} = (1 - \nu_{\theta_{\mathsf{UE}}})\sigma^2_\theta \tag{3.16}$$

$$\varepsilon^2_{\theta_{\mathsf{AP}}} = \mathsf{E}\{|\theta^{\mathsf{d}}_{B_m} - \theta^{\mathsf{u}}_{B_m}|^2\} = (1 - \nu_{\theta_{\mathsf{AP}}})\sigma^2_\theta \tag{3.17}$$

Specifically, we model the amplitude of the frequency responses { $A^d_{F_k}$ $A^u_{F_k}$ $A^d_{B_m}$ $A^u_{B_m}$ } as uniform random variables on the range$[1-\epsilon, 1+\epsilon]$, where e is chosen to set $\sigma^2_A = 0.01$.

In the case of the phase of the frequency responses { $\theta^d_{F_k}$ $\theta^u_{F_k}$ $\theta^d_{B_m}$ $\theta^u_{B_m}$ }, we choose a uniform distributed model on the range $[\pi, -\pi)$. This assumption imply a phase variance of

$$\sigma_\theta = \frac{(2\pi)^2}{12}\text{rad}^2 \tag{3.18}$$

In the worst case, when no correlation exists between the uplink and downlink channel, the root mean squared error is 104°.

3.2 Antenna mutual coupling

The performance of MIMO systems critically depends on the availability of independent channels between the transmitter and receiver. Correlation between channels downgrades the achievable capacity; this correlation is due to two components: spatial correlation and antenna mutual coupling [10, 54].

Many works show that wireless communication systems suffer from mutual coupling when the distance between antennas is small compared to the wavelength; this occurs because mutual coupling introduces spatial correlation [4].

Massive MIMO systems benefit from independent channels at each antenna to every user, for that reason, the antenna spacing chosen in massive MIMO is always greater than 0.5 λ which is a sufficient distance to obtain a low spatial correlation [21].

Even though the degradation produced by the effect of mutual coupling is assumable due to a significant separation between antennas, we also consider how a non-reciprocal response of mutual coupling affects system performance.

In this work, we do not analyse the overall effect of mutual antenna coupling on the performance of massive MIMO systems because it is a widely studied topic in literature and the impact is considerately small for treated antenna spacing distances, e.g. [1, 4, 16, 20, 21, 54].

In contrast with previous works [39, 40], we present analytical derivations for MRT precoder considering the effect of mutual coupling in both uplink and downlink.

When two antennas are very close compared to the wavelength, the electromagnetic field generated by one antenna affects the other antenna current distributions since in the near field of the transmitting antenna. On this basis, a voltage is induced at the non-transmitting antenna, and this is called mutual coupling [6].

Intending to quantify the mutual coupling, we define the mutual coupling impedance as the ratio between the induced voltage and current at the non-transmitting antenna given by [35]

$$z_{mn} = \frac{v_{mn}}{i_n} \tag{3.19}$$

where v_{mn} is the voltage induced at the antenna m by a current i_n at the antenna n.

$$V_{g,m} = (Z_L + Z_A)i_m + V_{ind,m} \tag{3.20}$$

where Z_L is the load impedance and $V_{ind,m}$ is the inducted voltage on the m-th antenna due to the current distributions of the rest of the antennas, which is given by [16, 53]

$$V_{ind,m} = \sum_{n \neq m}^{M} z_{mn} i_n \tag{3.21}$$

The generator voltage can be rewritten in matrix form as

$$\mathbf{V}_g = \mathbf{Z}\mathbf{i} \tag{3.22}$$

where $\mathbf{V}_g = [V_{g,1}, ..., V_{g,M}]^T$ generator voltage vector, $\mathbf{i} = [i_1, ..., i_M]^T$ is the current vector and the mutual impedance matrix $\mathbf{Z}$ is given by

$$\mathbf{Z} = \begin{bmatrix} Z_A + Z_L & Z_{12} & \dots & Z_{1M} \\ \vdots & \vdots & \ddots & \vdots \\ Z_{M1} & Z_{M2} & \dots & Z_A + Z_L \end{bmatrix}$$

Draw upon the mutual coupling impedance matrix; we obtain the coupling matrix by employing [21]

$$\mathbf{C} = (Z_A + Z_L)(\mathbf{Z} + Z_L \mathbf{I}_M)^{-1} \tag{3.23}$$

The coupling matrices in transmitting and receiving include a reciprocity error to model the non-reciprocal mutual coupling in a similar way as [38, 39, 40, 41, 58]

$$\mathbf{C}_t = \mathbf{C} + \mathbf{\Xi} \tag{3.24}$$

$$\mathbf{C}_r = \mathbf{C} \tag{3.25}$$

where $\mathbf{\Xi}$ is the reciprocity error matrix, and follows $\mathcal{CN}(0, \sigma^2_{MC})$.

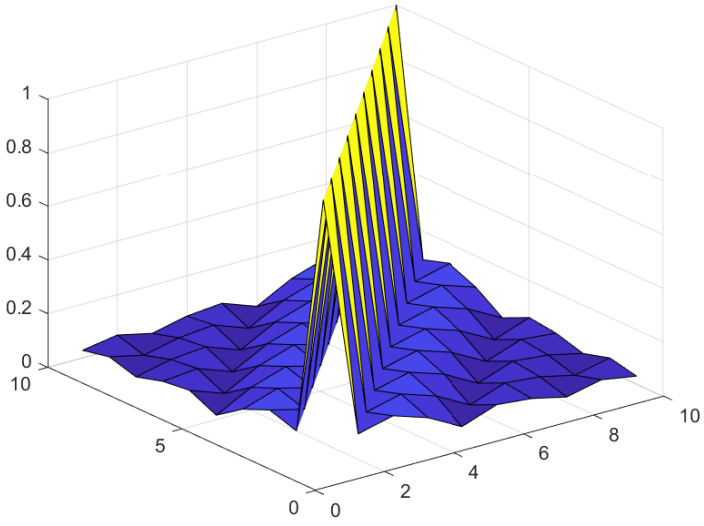

Figure 3.1. *Magnitude of the mutual coupling matrix for a collinear array of 10 antennas,* $l = \lambda/2$ *and* $d = \lambda/2$*.*

3.2.1 Wire dipole antenna array model

The impedance matrix depends on the specific array configuration, a collinear, rectangular or circular array of wire dipoles can be considered to model a realistic array disposition. The length of the dipole wire l is $\lambda/2$, obtaining a element impedance in isolation of $Z_A = 73 + j42.5\Omega$ [6]. The analytic expressions that model Z_{mn} can be obtained from [21, 50] and are given by

$$Z_{mn} = \begin{cases} 30(0.5772 + \ln(2kl) + C_i(2kl)) + j(30S_i(2kl)), & m = n \\ 30(2C_i(u_0) - C_i(u_1) - C_i(u_2)) - j(30(2S_i(u_0) - S_i(u_1) - S_i(u_2))), & m \neq n \end{cases}$$

where k is the wave number $2\pi/\lambda$, and

$$u_0 = kd_h \tag{3.26}$$

$$u_1 = k(\sqrt{d_h^2 + l^2} + l) \tag{3.27}$$

$$u_2 = k(\sqrt{d_h^2 + l^2} - l) \tag{3.28}$$

where d_h is the horizontal distance between the antennas, C_i and S_i are the cosine and sine integrals, respectively, given by

$$C_i(u) = \int_u^\infty \frac{cos(x)}{x} dx \tag{3.29}$$

$$S_i(u) = \int_0^u \frac{sin(x)}{x} dx \tag{3.30}$$

Note that when calculating Z_{mn}, the n-th dipole is assumed to be excited with current and the rest of the dipoles are open-circuited, hence the calculation of Z_{mn} assumes the presence of only two dipoles [7].

In Figure 3.1, the magnitude of the coupling matrix for an array of ten elements with linear geometry is shown, it is clear that as the distance between the elements increases, the mutual coupling impedance is reduced.

3.3 Overall system response

In our system model, we include the effects of hardware imperfections and mutual coupling, since the UEs are considered to be single-antenna the UE side does not take mutual coupling into account. The overall system response is then given by

$$\mathbf{H} = \mathbf{R}\mathbf{C}_r\mathbf{P}\mathbf{A} \tag{3.31}$$

$$\mathbf{G} = \mathbf{B}\mathbf{P}^{\mathsf{T}}\mathbf{C}_t\mathbf{T} \tag{3.32}$$

Note that in a fully distributed scenario, the coupling matrices are identity matrices. Thus there is no mutual coupling between APs and only the circuitry responses affect the performance.

3.4 Fast-varying and slow-varying non-reciprocal channel models

Most of the previous works and literature treat the non-reciprocity variables as fast-varying random variables, i.e. the values of the non-reciprocity variables change at a similar rate as the propagation channel. In this work, we present analytical derivations based on a slow-varying non-reciprocity parameters approach, considering a more physically-inspired and measurement-based non-reciprocity model [46]. Experimental results prove that reciprocity calibration can be repeated in the order of tens of minutes [46].

This slow/fast-varying difference can be seen as a comparison between the large and small-scale coefficients, where the large-scale coefficients usually follow a statistical model but they are considered constants in the expressions due to their slow variation rate.

Differences between models can be easily noticed when computing the statistical moments in the analytical derivations, e.g. in a fast-varying model the expected value reads $\mathrm{E}\{\mathbf{R}\} = \mu_R\mathbf{I}$ but conversely, in a slow-varying model the values are treated as unknown constants since they remain constant over many coherence intervals [46], hence

$\mathrm{E}\{\mathbf{R}\} = \mathbf{R}$. Those two different approaches lead to different simulation results; later on this work, we compare both approaches under certain conditions.

Let us present an example to prove how these approaches can differ, e.g. let p_{mk} denote the physical channel from the mth antenna to the kth user and t_m, r_m the transceiver responses in transmission and reception, respectively, at the transmitter.

The conjugate beamforming gain for fast and slow-varying models, respectively, are given by

$$\mathbb{E}\{|\sum_{m=1}^{M} p_{mk} t_m r_m^*|^2\} = \sum_{m=1}^{M} \mathbb{E}\{|p_{mk}|^2\}\mathbb{E}\{t_m r_m^*\} = \sum_{m=1}^{M} \mathbb{E}\{|p_{mk}|^2\} \tag{3.33}$$

$$\mathbb{E}\{|\sum_{m=1}^{M} p_{mk} t_m r_m^*\}|^2 = \sum_{m=1}^{M} \mathbb{E}\{|p_{mk}|^2\} t_m r_m^* \tag{3.34}$$

The beamforming gain in the fast-varying model does not depend on the transceiver frequency response since the expected value of the transceiver is to be reciprocal. On the contrary, the beamforming gain considering a slow-varying model depends on the actual values of the transceiver frequency responses realisation. One can notice that the phase reciprocity errors at the transmitter side impact the beamforming direction, i.e., the transmitted signals to the kth user do not add up coherently anymore, reducing the beamforming gain.

4 IMPACT OF CHANNEL NON-RECIPROCITY ON CELL-FREE MASSIVE MIMO SYSTEMS

4.1 Introduction

Classical cellular architectures divide the served area into different cells, and at each cell, one base station serves the users. When a device is at the cell edge suffers from very high interference due to neighbouring cells; thus, the performance drops [42]. Cell-Free systems propose to remove cells and operate using a massive number of access points spatially distributed over a large area serving a large number of users coherently. [30]

Cell-Free Massive MIMO, with a large number of distributed access points jointly serving a much smaller number of users in the same time-frequency resource, is a network architecture which promises to considerably improve the performance compared with conventional Massive MIMO centralised architectures [34].

Each access point acquires the channel state information through time-division duplex operation and the uplink pilots transmitted from the users. The access points rely on channel reciprocity to directly use the uplink channel estimate as downlink channel estimate and perform the beamforming [31].

Cell-Free term means that all antennas are not collocated in a single base station located at the centre of the cell, but the antennas are spatially dispersed over different APs. The main advantage of Cell-Free massive MIMO architectures is the spatial diversity, i.e. the distance between the users and the nearest AP is reduced [30], a CF massive MIMO deployment provides a more uniform coverage to users at random locations than the classical centralised massive MIMO cells [34].

Cell-Free Massive MIMO systems are different from previous distributed Massive MIMO in the sense that Cell-Free systems serve all the users independently of their location and the distributed Massive MIMO systems only serve the users that are at its cell.

A central processing unit (CPU) controls all the APs, providing the data payload and signalling needed for a synchronised transmission from the APs to the users [30, 31, 34]. All the protocols between APs and CPU are excluded from this work, considering a perfect and error-free backhaul with unlimited capacity.

The DL-UL transmission proceeds by TDD mode and each coherence interval is divided

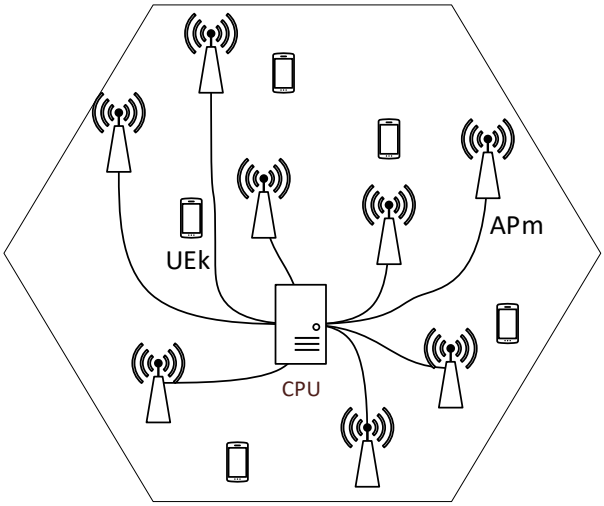

Figure 4.1. *Overview of Cell-Free architecture.*

into three stages: uplink training, downlink payload data transmission and uplink payload data transmission [30, 32].

4.2 Model description

Let L, M and K be the number of APs, antenna elements per AP and number of users, respectively, with $LM >> K$.

We consider a standard frequency-flat block fading channel model between the APs and the UEs [31, 34]. Thus the channel matrix is assumed to be constant within the coherence interval of τ symbols.

Let us denote $\mathbf{H}_l \triangleq [\mathbf{h}_{l,1}, ..., \mathbf{h}_{l,K}]$ as the $M \times K$ uplink channel matrix between the UEs and the lth AP, where $\mathbf{h}_{l,k}$ denotes the $M \times 1$ vector channel between the kth UE and the M antennas at the lth AP. The total channel matrix between the K UEs and the LM antenna elements is defined as $\mathbf{H} \triangleq [\mathbf{H}_1^T, ..., \mathbf{H}_L^T]^T$.

The uplink channel vector from the kth user to the lth AP is given by

$$\mathbf{h}_{l,k} = a_k \mathbf{R}_l \mathbf{C}_{r,l} \mathbf{p}_{l,k} \tag{4.1}$$

where $\mathbf{p}_{l,k} \sim \mathcal{CN}(0, \beta_{l,k}\mathbf{I}_M)$ is the physical propagation channel with i.i.d entries and $\beta_{l,k}$ is the large scale coefficient between the kth UE and the lth AP, a_k is the frequency response of the kth UE transmitter, $\mathbf{R}_l$ is the $M \times M$ diagonal matrix of frequency responses at the lth AP receivers and $\mathbf{C}_{r,l}$ is the $M \times M$ receiver mutual coupling matrix at the lth AP.

The different channels between the kth user and the M antennas at the lth AP are not independent any more. We define the covariance matrix of the channel vector between the kth user and the lth AP as

$$\mathbf{\Delta}_{l,k}^{\mathsf{u}} \triangleq \mathbb{E}\{||\mathbf{h}_{l,k}||^2\} = |a_k|^2 \beta_k^{(l)} \mathbf{R}_l \mathbf{C}_{\mathsf{RX},l} \mathbf{C}_{\mathsf{RX},l}^{\dagger} \mathbf{R}_l^{\dagger} \tag{4.2}$$

We can assume total statistical independence between the channels at different APs, hence the kth column of the total channel matrix $\mathbf{H}$ follows $\mathbf{h}_k \sim \mathcal{CN}(0, \mathbf{\Delta}_k^{\mathsf{u}})$ where $\mathbf{\Delta}_k =$ blckdiag$(\mathbf{\Delta}_{1,k}^{\mathsf{u}}, ..., \mathbf{\Delta}_{L,k}^{\mathsf{u}})$.

Similarly, we can define the downlink channel vector from the kth user to the lth AP as

$$\mathbf{g}_{l,k} = b_k \mathbf{T}_l \mathbf{C}_{\mathsf{TX},l} \mathbf{p}_{l,k} \tag{4.3}$$

where b_k is the frequency response of the kth UE receiver, $\mathbf{T}_l$ is the $M \times M$ diagonal matrix of frequency responses at the lth AP transmitters and $\mathbf{C}_{t,l}$ is the $M \times M$ transmitter mutual coupling matrix at the lth AP.

The covariance matrix of the downlink channel vector from the kth user at the lth AP is given by

$$\mathbf{\Delta}_{l,k}^{\mathsf{d}} \triangleq \mathbb{E}\{||\mathbf{g}_{l,k}||^2\} = |b_k|^2 \beta_k^{(l)} \mathbf{T}_l \mathbf{C}_{t,l} \mathbf{C}_{t,l}^{\dagger} \mathbf{T}_l^{\dagger} \tag{4.4}$$

From the equations (4.3) and (4.1), we derive the relation between downlink and uplink channels as

$$\mathbf{g}_{l,k} = \frac{b_k}{a_k} \mathbf{T}_l \mathbf{C}_{t,l} \mathbf{R}_l^{-1} \mathbf{C}_{r,l}^{-1} \mathbf{h}_{l,k} = \mathbf{E}_{l,k} \mathbf{h}_{l,k} \tag{4.5}$$

where $\mathbf{E}_{l,k}$ is the $M \times M$ reciprocal error matrix at the lth AP and kth user.

4.2.1 Uplink pilots and channel estimation

At the beginning of each coherence interval, a set of pilot waveforms must be transmitted from the UEs to the APs to estimate the channels between every antenna and user, and not to interfere they have to be mutually orthogonal [25]. In case that no pilot contamination is considered the length of the pilot sequence is τ_p and $\tau_c \geq \tau_p \geq K$, but if there are not enough orthogonal pilot sequences available for all the users then $\tau_c \geq K \geq \tau_p$ and there is pilot contamination since the channel estimates of certain users interfere [14].

We denote the pilot sequence assigned to the kth user as a $\tau_p \times 1$ vector $\boldsymbol{\varphi}_k$, and the $\tau_p \times \tau_p$ matrix grouping all the sequences holds [25]

$$\mathbf{\Phi}^H \mathbf{\Phi} = \mathbf{I}_{\tau_p} \tag{4.6}$$

The sequence transmitted from the kth user is a $\tau_p \times 1$ sequence given by

$$\mathbf{x}_{p,k} = \sqrt{\rho_u \tau_p} \boldsymbol{\varphi}_k^* \tag{4.7}$$

where the energy transmitted depends on the length of the pilot sequence.

To perform the channel estimation, all the UEs simultaneously transmit the UL pilot sequences assigned by the CPU. The received signal at the lth AP by its mth antenna reads

$$\mathbf{y}_{p,l,m} = \sqrt{\rho_u \tau_p} \sum_{k=1}^{K} h_{l,m,k} \boldsymbol{\varphi}_k^* + \mathbf{n}_{p,l,m} \tag{4.8}$$

where $\mathbf{n}_{p,l,m}$ are i.i.d $\mathcal{CN}(0,1)$ RVs representing the thermal noise.

The lth AP receives a set of $\tau_p \times M$ signals defined as $\mathbf{Y}_{p,l} = [\mathbf{y}_{p,l,1}, ..., \mathbf{y}_{p,l,M}]$, and each AP de-spreads the received set of signals by projecting over the pilot sequences, obtaining samples proportional to the channel from the AP to the kth user. The de-spread $M \times 1$ signal of the kth user yields

$$\check{\mathbf{y}}_{p,l,k} = \mathbf{y}_{p,l,k}^T \boldsymbol{\varphi}_k = \sqrt{\tau_p \rho_u} \mathbf{h}_{l,k} + \sqrt{\tau_p \rho_u} \sum_{k' \neq k}^{K} \mathbf{h}_{l,k'} \boldsymbol{\varphi}_{k'}^H \boldsymbol{\varphi}_k + \check{\mathbf{n}}_{p,l,m} \tag{4.9}$$

The linear MMSE estimator or Wiener filter of $\mathbf{x}$ from $\mathbf{y}$ is given by [19]

$$\hat{\mathbf{x}} = \mathbf{m}_x + \boldsymbol{\Sigma}_{x,y} \boldsymbol{\Sigma}_y^{-1} (\mathbf{y} - \mathbf{m}_y) \tag{4.10}$$

where $\mathbf{m}_x$ and $\mathbf{m}_y$ are the mean vectors of $\mathbf{x}$ and $\mathbf{y}$, respectively, $\boldsymbol{\Sigma}_{x,y}$ is the covariance matrix between $\mathbf{x}$ and $\mathbf{y}$ and $\boldsymbol{\Sigma}_y$ is the auto-covariance matrix of $\mathbf{y}$. Thus, the linear MMSE channel estimate of $\mathbf{h}_{l,k}$ is given by

$$\hat{\mathbf{h}}_{l,k} = \sqrt{\rho_u \tau_u} \boldsymbol{\Delta}_{l,k}^{\mathsf{u}} (\rho_u \tau_u \boldsymbol{\Delta}_{l,k}^{\mathsf{u}} + \rho_u \tau_u \sum_{k' \neq k}^{K} \boldsymbol{\Delta}_{l,k'}^{\mathsf{u}} \boldsymbol{\varphi}_{k'}^H \boldsymbol{\varphi}_k + \mathbf{I}_M)^{-1} \check{\mathbf{y}}_{p,l,k} \tag{4.11}$$

The corresponding uplink channel estimate covariance $M \times M$ matrix of $\hat{\mathbf{h}}_{l,k}$, denoted by $\boldsymbol{\Phi}_{l,k}$, reads

$$\boldsymbol{\Phi}_{l,k} = \mathbb{E}\{\hat{\mathbf{h}}_{l,k} \hat{\mathbf{h}}_{l,k}^H\} = \rho_u \tau_u \boldsymbol{\Delta}_{l,k}^{\mathsf{u}} (\rho_u \tau_u \boldsymbol{\Delta}_{l,k}^{\mathsf{u}} + \rho_u \tau_u \sum_{k' \neq k}^{K} \boldsymbol{\Delta}_{l,k'}^{\mathsf{u}} \boldsymbol{\varphi}_{k'}^H \boldsymbol{\varphi}_k + \mathbf{I}_M)^{-1} \boldsymbol{\Delta}_{l,k}^{\mathsf{u}} \tag{4.12}$$

During this work, we focus on the impact of non-reciprocal responses. Hence, we do not consider pilot contamination in our analysis, the covariance matrix of the uplink channel estimate yields

$$\boldsymbol{\Phi}_{l,k} = \mathbb{E}\{\hat{\mathbf{h}}_{l,k} \hat{\mathbf{h}}_{l,k}^H\} = \rho_u \tau_u \boldsymbol{\Delta}_{l,k}^{\mathsf{u}} (\rho_u \tau_u \boldsymbol{\Delta}_{l,k}^{\mathsf{u}} + \mathbf{I}_M)^{-1} \boldsymbol{\Delta}_{l,k}^{\mathsf{u}} \tag{4.13}$$

4.2.2 Downlink data transmission

Considering an NRC-unaware case, the APs rely on channel reciprocity and use the uplink channel estimate as true downlink channel estimate. The transmitted signal from

the lth AP is given by

$$\mathbf{x}_l = \sqrt{\rho_d} \sum_{k=1}^{K} \sqrt{\eta_{l,k}} \mathbf{w}_{l,k} q_k \tag{4.14}$$

where ρ_d corresponds with the normalized downlink transmit SNR, $\eta_{l,k}$ is the power control coefficient at the lth AP to the kth user, $\mathbf{w}_{l,k}$ is the $M \times 1$ precoding vector at the lth AP to the kth user and q_k is the symbol intended for the kth user and $\mathbf{q} = [q_1, ..., q_K]^T$ holds $\mathbb{E}\{\mathbf{q}\mathbf{q}^H\} = \mathbf{I}_K$.

Therefore, the received signal at the kth user can be expressed as

$$y_k = \sqrt{\rho_d} \sum_{l=1}^{L} \sqrt{\eta_{l,k}} \mathbf{g}_{l,k}^T \mathbf{w}_{l,k} q_k + \sqrt{\rho_d} \sum_{k' \neq k}^{K} \sum_{l=1}^{L} \sqrt{\eta_{l,k}} \mathbf{g}_{l,k}^T \mathbf{w}_{l,k'} q_{k'} + n_k \tag{4.15}$$

where $w_k \backsim \mathcal{CN}(0, 1)$ denotes receiver thermal noise with variance normalized to one.

Classical Massive MIMO systems rely on channel hardening when detecting the received signal, i.e. users rely on the channel statistic properties of the desired term to detect the symbol [8]. Based on (4.15), we define the strength of the desired signal based on the channel statistic properties as

$$\mathsf{DS}_k = \sqrt{\rho_d} \sum_{l=1}^{L} \sqrt{\eta_{l,k}} \mathbb{E}\{\mathbf{g}_{l,k}^T \mathbf{w}_{l,k}\} \tag{4.16}$$

The lack of knowledge of the effective instantaneous channel, $\mathbf{g}_{l,k}^T \mathbf{w}_{l,k}$, is captured by the beamforming gain uncertainty or self-interference given by

$$\mathsf{BU}_k = \sqrt{\rho_d} \sum_{l=1}^{L} \sqrt{\eta_{l,k}} (\mathbf{g}_{l,k}^T \mathbf{w}_{l,k} - \mathbb{E}\{\mathbf{g}_{l,k}^T \mathbf{w}_{l,k}\}) \tag{4.17}$$

One can notice that if the variance of the effective channel gain is relatively small, there is no large improvement when the user knows the exact channel gain, but if the channel does not harden, we will underestimate the achievable rate.

Since K users are sharing the same time-frequency resources; if the channel is not orthogonal, there is also interference between users that degrades the performance. Let us define this interference known as channel non-orthogonality or inter-user interference as

$$\mathsf{IUI}_{k,k'} = \sqrt{\rho_d} \sum_{l=1}^{L} \sqrt{\eta_{l,k'}} \mathbf{g}_{l,k}^T \mathbf{w}_{l,k'} \tag{4.18}$$

The received signal at the kth user then reads

$$y_k = \mathsf{DS}_k \cdot q_k + \mathsf{BU}_k \cdot q_k + \sum_{k' \neq k}^{K} \mathsf{IUI}_{k,k'} \cdot q_{k'} + n_k \tag{4.19}$$

Achievable rate

The so-called Use-and-then-Forget is a simple lower bound, which in most centralised Massive MIMO cases is tight. This bound is computed using the effective SINR as

$$R_k^{\mathsf{UatF}} = \log_2(1 + \mathsf{SINR}_k) \tag{4.20}$$

where SINR_k, considering the interference terms as uncorrelated effective noise, is defined as follows

$$\mathsf{SINR}_k = \frac{\mathbb{E}\{|\mathsf{DS}_k|^2\}}{\mathbb{E}\{|\mathsf{BU}_k|^2\} + \sum_{k' \neq k}^{K} \mathbb{E}\{|\mathsf{IUI}_{k,k'}|^2\} + 1} \tag{4.21}$$

Conversely, the genie-aided bound is based on the fact that the user knows exactly the effective channel gain when detecting the received symbol. This case is not practically feasible, but we can extract some insights from the analysis to be used in later works. The bound is defined as follows

$$R_k^{\mathsf{GA}} = \log_2\left(1 + \frac{\mathbb{E}\{|\mathsf{DS}_k|^2\} + \mathbb{E}\{|\mathsf{BU}_k|^2\}}{\sum_{k' \neq k}^{K} \mathbb{E}\{|\mathsf{IUI}_{k,k'}|^2\} + 1}\right) \tag{4.22}$$

It is well-known from the literature that under certain conditions when a sufficient large number of antennas is used, the UatF bound approximates the genie-aided bound [8, 25].

Maximum ratio transmission or conjugate beamforming

The aim of the maximum-ratio precoding is combine coherently all the transmitted signals from the LM antennas at the kth user, amplifying the desired signal as much as possible, but disregarding the interference from other users. If only one terminal were transmitting, this would be the optimal precoding scheme.

The precoding vector intended for the kth user at the lth AP can be expressed as

$$\mathbf{w}_{l,k} = \hat{\mathbf{h}}_{l,k}^{*} \tag{4.23}$$

Let us calculate an useful statistic of the MRT precoder used throughout the analytical derivations as

$$\mathbb{E}\{||\mathbf{w}_{l,k}||^2\} = \mathsf{tr}(\boldsymbol{\Phi}_{\boldsymbol{l},\boldsymbol{k}}) \tag{4.24}$$

If we substitute the precoder vector from (4.23) in (4.16), the desired signal strength reads

$$
\begin{aligned}
\mathsf{DS}_k &= \sqrt{\rho_d}\sum_{l=1}^{L}\sqrt{\eta_{l,k}}\mathbb{E}\{\mathbf{g}_{l,k}^T\hat{\mathbf{h}}_{l,k}^*\} \\
&= \sqrt{\rho_d}\sum_{l=1}^{L}\sqrt{\eta_{l,k}}\mathbb{E}\{\mathbf{h}_{l,k}^T\mathbf{E}_{l,k}\hat{\mathbf{h}}_{l,k}^*\} \\
&= \sqrt{\rho_d}\sum_{l=1}^{L}\sqrt{\eta_{l,k}}(\mathbb{E}\{\hat{\mathbf{h}}_{l,k}^T\mathbf{E}_{l,k}\hat{\mathbf{h}}_{\}}^* + \mathbb{E}\{\tilde{\mathbf{h}}_{l,k}^T\mathbf{E}_{l,k}\hat{\mathbf{h}}_{l,k}^*\}) \\
&= \sqrt{\rho_d}\sum_{l=1}^{L}\sqrt{\eta_{l,k}}\mathsf{tr}(\mathbf{E}_{l,k}\boldsymbol{\Phi}_{\boldsymbol{l},\boldsymbol{k}})
\end{aligned}
\tag{4.25}
$$

The beamforming uncertainty is computed based on the previous result as

$$
\begin{aligned}
\mathbb{E}\{|\mathsf{BU}_k|^2\} &= \rho_d\mathbb{E}\{|\sum_{l=1}^{L}\eta_{l,k}\mathbf{g}_{l,k}^T\mathbf{w}_{l,k}|^2\} - \rho_d|\sum_{l=1}^{L}\eta_{l,k}\mathbb{E}\{\mathbf{g}_{l,k}^T\mathbf{w}_{l,k}\}|^2 \\
&= \rho_d\sum_{l=1}^{L}\eta_{l,k}(\mathbb{E}\{|\mathbf{g}_{l,k}^T\mathbf{w}_{l,k}|^2\} - |\mathbb{E}\{\mathbf{g}_{l,k}^T\mathbf{w}_{l,k}\}|^2) \\
&= \rho_d\sum_{l=1}^{L}\eta_{l,k}(\mathbb{E}\{|\hat{\mathbf{h}}_{l,k}^T\mathbf{E}_{l,k}\hat{\mathbf{h}}_{l,k}^*|^2\} + \mathbb{E}\{|\tilde{\mathbf{h}}_{l,k}^T\mathbf{E}_{l,k}\hat{\mathbf{h}}_{l,k}^*|^2\} \\
&- |\mathbb{E}\{\mathbf{g}_{l,k}^T\mathbf{w}_{l,k}\}|^2) \\
&= \rho_d\sum_{l=1}^{L}\eta_{l,k}(\mathsf{tr}(\mathbf{E}_{l,k}^*\boldsymbol{\Phi}_{\boldsymbol{l},\boldsymbol{k}}\mathbf{E}_{l,k}\boldsymbol{\Phi}_{\boldsymbol{l},\boldsymbol{k}}) + |\mathsf{tr}(\mathbf{E}_{l,k}\boldsymbol{\Phi}_{\boldsymbol{l},\boldsymbol{k}})|^2 \\
&+ \mathsf{tr}(\mathbf{E}_{l,k}^*\boldsymbol{\Phi}_{\boldsymbol{l},\boldsymbol{k}}\mathbf{E}_{l,k}(\boldsymbol{\Delta}_{\boldsymbol{l},\boldsymbol{k}} - \boldsymbol{\Phi}_{\boldsymbol{l},\boldsymbol{k}})) - |\mathbb{E}\{\mathbf{g}_{l,k}^T\mathbf{w}_{l,k}\}|^2) \\
&= \rho_d\sum_{l=1}^{L}\eta_{l,k}\mathsf{tr}(\mathbf{E}_A^{(l)*}\boldsymbol{\Phi}_{\boldsymbol{l},\boldsymbol{k}}\mathbf{E}_{l,k}\boldsymbol{\Delta}_{\boldsymbol{l},\boldsymbol{k}})
\end{aligned}
\tag{4.26}
$$

The interference term from every user is calculated as follows

$$
\begin{aligned}
\mathbb{E}\{|\mathsf{IUI}_{k,k'}|^2\} &= \rho_d\mathbb{E}\{|\sum_{l=1}^{L}\eta_{l,k}\mathbf{g}_{l,k}^T\mathbf{w}_{l,k'}|^2\} \\
&= \rho_d\sum_{l=1}^{L}\eta_{l,k}\mathbb{E}\{|\mathbf{g}_{l,k}^T\mathbf{w}_{l,k'}|^2\} \\
&= \rho_d\sum_{l=1}^{L}\eta_{l,k}(\mathbb{E}\{|\hat{\mathbf{h}}_{l,k}^T\mathbf{E}_{l,k}\hat{\mathbf{h}}_{l,k'}^*|^2\} + \mathbb{E}\{|\tilde{\mathbf{h}}_{l,k}^T\mathbf{E}_{l,k}\hat{\mathbf{h}}_{l,k'}^*|^2\}) \\
&= \rho_d\sum_{l=1}^{L}\eta_{l,k}(\mathsf{tr}(\mathbf{E}_{l,k}^*\boldsymbol{\Phi}_{\boldsymbol{l},\boldsymbol{k}}\mathbf{E}_{l,k}\boldsymbol{\Phi}_{\boldsymbol{l},\boldsymbol{k'}}) + \mathsf{tr}(\mathbf{E}_{l,k}^*\boldsymbol{\Phi}_{\boldsymbol{l},\boldsymbol{k'}}\mathbf{E}_{l,k}(\boldsymbol{\Delta}_{\boldsymbol{l},\boldsymbol{k}} - \boldsymbol{\Phi}_{\boldsymbol{l},\boldsymbol{k}}))) \\
&= \rho_d\sum_{l=1}^{L}\eta_{l,k}\mathsf{tr}(\mathbf{E}_{l,k}^*\boldsymbol{\Phi}_{\boldsymbol{l},\boldsymbol{k'}}\mathbf{E}_{l,k}\boldsymbol{\Delta}_{\boldsymbol{l},\boldsymbol{k}})
\end{aligned}
\tag{4.27}
$$

The denominator of the SINR expression is compound by the beamforming uncertainty and the interference from the rest of the users, given by

$$\mathbb{E}\{|\mathsf{BU}_k|^2\} + \sum_{k' \neq k}^{K} \mathbb{E}\{|\mathsf{IUI}_{k,k'}|^2\} = \rho_d \sum_{k'=1}^{K} \sum_{l=1}^{L} \eta_{l,k} \mathsf{tr}(\mathbf{E}_{l,k}^{*} \boldsymbol{\Phi}_{\boldsymbol{l},\boldsymbol{k'}} \mathbf{E}_{l,k} \boldsymbol{\Delta}_{\boldsymbol{l},\boldsymbol{k}}) \tag{4.28}$$

The final SINR expression reads

$$\mathsf{SINR}_k = \frac{\rho_d |\sum_{l=1}^{L} \sqrt{\eta_{l,k}} \mathsf{tr}(\mathbf{E}_{l,k} \boldsymbol{\Phi}_{\boldsymbol{l},\boldsymbol{k}})|^2}{\rho_d \sum_{l=1}^{L} \sum_{k'=1}^{K} \eta_{l,k'} \cdot \mathsf{tr}(\mathbf{E}_{l,k}^{*} \boldsymbol{\Phi}_{\boldsymbol{l},\boldsymbol{k'}} \mathbf{E}_{l,k} \boldsymbol{\Delta}_{\boldsymbol{l},\boldsymbol{k}}) + 1} \tag{4.29}$$

These expressions capture the effects of uplink based channel estimation and mutual coupling between antennas as well as the non-reciprocity due to transceiver frequency response and mutual coupling mismatches.

In the case of reciprocal transceiver responses, the effective signal-to-noise ratio reads

$$\mathsf{SINR}_k = \frac{\rho_d |\sum_{l=1}^{L} \sqrt{\eta_{l,k}} \mathsf{tr}(\boldsymbol{\Phi}_{\boldsymbol{l},\boldsymbol{k}})|^2}{\rho_d \sum_{l=1}^{L} \sum_{k'=1}^{K} \eta_{l,k'} \mathsf{tr}(\boldsymbol{\Phi}_{\boldsymbol{l},\boldsymbol{k'}} \boldsymbol{\Delta}_{\boldsymbol{l},\boldsymbol{k}}) + 1} \tag{4.30}$$

In the case of ideal transceiver responses, the effective signal-to-noise ratio yields

$$\mathsf{SINR}_k = \frac{\rho_d M^2 |\sum_{l=1}^{L} \sqrt{\eta_{l,k}} \phi_{l,k}|^2}{\rho_d M \sum_{l=1}^{L} \sum_{k'=1}^{K} \eta_{l,k'} \phi_{l,k'} \beta_{l,k} + 1} \tag{4.31}$$

where $\phi_{l,k}$ is the variance of the channel estimates at the lth AP from the kth user. In this case, no mutual coupling or transceiver responses are considered, only the physical propagation channel is taken into account.

Zero-forcing precoder

The aim of the zero-forcing precoding is to suppress the inter-user interference, ZF precoder and its implications are briefly described in chapter 2.

Implementing ZF precoding requires exchanging instantaneous CSI between APs and the CPU, that implies considerable front-haul traffic and an unscalable architecture if the number of APs grows. For that reason, we use a similar approach as [18], where each AP is equipped with a sufficient number of antennas to perform its beamforming.

To achieve mathematical tractability in this problem, we have to take some assumptions as previous works considered [39, 40]. In particular, we are assuming that there is no mutual coupling in the uplink channel, and the non-reciprocal matrix error captures the mutual coupling effect. That allows us to obtain analytical derivations and extract insight from the results.

Essentially, we model both uplink and downlink transceiver and mutual coupling responses

and we obtain the reciprocity matrix error which captures the difference between uplink and downlink channels.

Let us define the uplink channel for this case as

$$\mathbf{h}_{l,k} = \mathbf{p}_{l,k} \tag{4.32}$$

The downlink channel captures the non-reciprocity effect as follows

$$\mathbf{g}_{l,k} = \mathbf{E}_{l,k}\mathbf{p}_{l,k} \tag{4.33}$$

where $\mathbf{E}_{l,k}$ is given by

$$\mathbf{E}_{l,k} = \frac{b_k}{a_l}\mathbf{T}_l\mathbf{C}_{\mathsf{TX},l}\mathbf{R}_l^{-1}\mathbf{C}_{\mathsf{RX},l}^{-1} \tag{4.34}$$

It might not be the optimal approach, but as previous works argued, it is a plausible solution to a complex mathematical problem.

We define the precoder vector intended for the kth user as

$$\mathbf{w}_{l,k} = \hat{\mathbf{H}}_l^H(\hat{\mathbf{H}}_l\hat{\mathbf{H}}_l^H)^{-1}\mathbf{e}_k \tag{4.35}$$

As in the MRT section, we need to calculate an useful statistic given by

$$\mathbb{E}\{||\mathbf{w}_{l,k}||^2\}^{-1} = \phi_{l,k}(M-K) \tag{4.36}$$

Next, we derive two useful properties that we use further on. Firstly, let us define **Property 1** as the expected value of the product of the precoder elements and the channel is obtained as

$$\mathbb{E}\{\hat{\mathbf{h}}_{l,k}^T\mathbf{w}_{l,k}\} = 1 \implies \mathbb{E}\{\hat{h}_{l,m,k}w_{l,m,k}\} = \frac{1}{M} \tag{4.37}$$

Secondly, let us define **Property 2** as the power of the precoder elements is obtained by using the inverse Wishart matrix properties as follows [25, 49]

$$\mathbb{E}\{||\mathbf{w}_{l,k}||^2\}^{-1} = \phi_{l,k}(M-K) \implies \mathbb{E}\{|w_{l,m,k}|^2\} = \frac{1}{\phi_{l,k}M(M-K)} \tag{4.38}$$

Based on Property 1 and assuming $\mathbb{E}\{w_{l,m,k}h_{l,n,k}\} = 0, m \neq n$, the strength of the desired

signal reads

$$\begin{aligned}\mathsf{DS}_k &= \sqrt{\rho_d}\sum_{l=1}^{L}\sqrt{\eta_{l,k}}\mathbb{E}\{\mathbf{g}_{l,k}^T\mathbf{w}_{l,k}^*\} \\ &= \sqrt{\rho_d}\sum_{l=1}^{L}\sqrt{\eta_{l,k}}\sum_{m=1}^{M}\sum_{n=1}^{M}\mathbb{E}\{w_{l,m,k}h_{l,n,k}\}e_{mn} \\ &= \sqrt{\rho_d}\sum_{l=1}^{L}\sqrt{\eta_{l,k}}\frac{\mathsf{tr}(\mathbf{E}_{l,k})}{M}\end{aligned} \tag{4.39}$$

Since the variance of a sum of independent random variables is equal to the sum of the variances, we have

$$\mathbb{E}\{|\mathsf{BU}_k|^2\} = \rho_d\mathsf{Var}\left(\sum_{l=1}^{L}\sqrt{\eta_{l,k}}\mathbf{g}_{l,k}^T\mathbf{w}_{l,k}\right) = \rho_d\sum_{l=1}^{L}\eta_{l,k}\mathsf{Var}(\mathbf{g}_{l,k}^T\mathbf{w}_{l,k}) \tag{4.40}$$

We derive the variance of the beamformed signal at the lth AP separately as

$$\mathsf{Var}(\mathbf{g}_{l,k}^T\mathbf{w}_{l,k}) = \mathsf{Var}(\mathbf{h}_{l,k}^T\mathbf{E}_{l,k}\mathbf{w}_{l,k}) = \mathbb{E}\{|\mathbf{h}_{l,k}^T\mathbf{E}_{l,k}\mathbf{w}_{l,k}|^2\} - |\mathbb{E}\{\mathbf{h}_{l,k}^T\mathbf{E}_{l,k}\mathbf{w}_{l,k}\}|^2 \tag{4.41}$$

Since channel estimate and channel estimation error are uncorrelated and zero mean

$$\mathbb{E}\{|\mathbf{h}_{l,k}^T\mathbf{E}_{l,k}\mathbf{w}_{l,k}|^2\} = \mathbb{E}\{|\hat{\mathbf{h}}_{l,k}^T\mathbf{E}_{l,k}\mathbf{w}_{l,k}|^2\} + \mathbb{E}\{|\tilde{\mathbf{h}}_{l,k}^T\mathbf{E}_{l,k}\mathbf{w}_{l,k}|^2\} \tag{4.42}$$

The channel estimation error $\tilde{\mathbf{h}}_{l,k}$ and the precoder vector $\mathbf{w}_{l,k}$ are uncorrelated, hence the statistical crossed term is given by

$$\mathbb{E}\{|\tilde{\mathbf{h}}_{l,k}^T\mathbf{E}_{l,k}\mathbf{w}_{l,k}|^2\} = (\beta_{l,k}-\phi_{l,k})\mathbb{E}\{\mathbf{w}_{l,k}^\dagger\mathbf{E}_{l,k}^\dagger\mathbf{E}_{l,k}\mathbf{w}_{l,k}\} = \frac{(\beta_{l,k}-\phi_{l,k})}{\phi_{l,k}M(M-K)}\mathsf{tr}(\mathbf{E}_{l,k}^\dagger\mathbf{E}_{l,k}) \tag{4.43}$$

The same result is obtained for the inter-user interference

$$\begin{aligned}\mathbb{E}\{|\tilde{\mathbf{h}}_{l,k}^T\mathbf{E}_{l,k}\mathbf{w}_{l,k'}|^2\} &= (\beta_{l,k}-\phi_{l,k})\mathbb{E}\{\mathbf{w}_{l,k'}^\dagger\mathbf{E}_{l,k}^\dagger\mathbf{E}_{l,k}\mathbf{w}_{l,k'}\} \\ &= \frac{(\beta_{l,k}-\phi_{l,k})}{\phi_{l,k'}M(M-K)}\mathsf{tr}(\mathbf{E}_{l,k}^\dagger\mathbf{E}_{l,k})\end{aligned} \tag{4.44}$$

We separate the non-reciprocity error matrix as $\mathbf{E}_{l,k} = \mathbf{I}+\mathbf{E}'_{l,k}$ and we obtain the statistical moments as follows

$$\mathbb{E}\{|\hat{\mathbf{h}}_{l,k}^T\mathbf{E}_{l,k}\mathbf{w}_{l,k}|^2\} = 1 + \mathbb{E}\{|\hat{\mathbf{h}}_{l,k}^T\mathbf{E}'_{l,k}\mathbf{w}_{l,k}|^2\} + \frac{2Re\{\mathsf{tr}(\mathbf{E}_{l,k})\}}{M} \tag{4.45}$$

$$|\mathbb{E}\{\hat{\mathbf{h}}_{l,k}^T\mathbf{E}_{l,k}\mathbf{w}_{l,k}\}|^2 = 1 + \frac{|\mathsf{tr}(\mathbf{E}'_{l,k})|^2}{M^2} + \frac{2Re\{\mathsf{tr}(\mathbf{E}_{l,k})\}}{M} \tag{4.46}$$

$$\text{Var}(\mathbf{h}_{l,k}^T \mathbf{E}_{l,k} \mathbf{w}_{l,k}) = \mathbb{E}\{|\hat{\mathbf{h}}_{l,k}^T \mathbf{E}'_{l,k} \mathbf{w}_{l,k}|^2\} - \frac{|\text{tr}(\mathbf{E}'_{l,k})|^2}{M^2} + \mathbb{E}\{|\tilde{\mathbf{h}}_{l,k}^T \mathbf{E}_{l,k} \mathbf{w}_{l,k}|^2\} \tag{4.47}$$

In order to obtain analytical derivations, we use an approximation of the ZF precoder elements based on massive MIMO concepts. Taking the following product matrix $\hat{\mathbf{H}}_l \hat{\mathbf{H}}_l^\dagger$ and relying on favourable propagation we assume the following [27]

$$\hat{\mathbf{h}}_{l,k}^H \hat{\mathbf{h}}_{l,k'} \approx \begin{cases} M \cdot \phi_{l,k} & \text{if } k = k' \\ 0 & \text{if } k \neq k' \end{cases}$$

Hence, the matrix product can be approximated as $\hat{\mathbf{H}}_l \hat{\mathbf{H}}_l^\dagger \approx M \cdot \phi_{l,k} \mathbf{I}_K$, and the elements of the precoder $\hat{\mathbf{H}}_l^\dagger (\hat{\mathbf{H}}_l \hat{\mathbf{H}}_l^\dagger)^{-1}$ are approximated as

$$w_{l,m,k} \approx \frac{\hat{h}_{l,m,k}^*}{M \phi_{l,k}} \tag{4.48}$$

To the best of our knowledge, this approximation has only been used in [27]. Other works as [5, 40] approximated as

$$\mathbf{w}_{l,k} \approx c \hat{h}_{l,m,k}^* \tag{4.49}$$

where c is obtained by solving the power constraint at the AP. We decided to use the massive MIMO inspired approach because it obtained more accurate results than the other approach.

Built upon this approximation, we derive expressions for the statistical moments. First, we consider the power of the intended signal for the kth user

$$\begin{aligned}
\mathbb{E}\{|\hat{\mathbf{h}}_{l,k}^T \mathbf{E}'_{l,k} \mathbf{w}_{l,k}|^2\} &= \mathbb{E}\{|\sum_{m=1}^{M} \sum_{n=1}^{M} \hat{h}_{l,m,k} e'_{l,k,mn} w_{l,n,k}|^2\} \\
&= \mathbb{E}\{\sum_{m=1}^{M} \sum_{n=1}^{M} \sum_{m'=1}^{M} \sum_{n'=1}^{M} \hat{h}_{l,m,k} e'_{l,k,mn} w_{l,n,k} \hat{h}_{l,m',k}^* e'^*_{l,k,m'n'} w_{l,n',k}^*\} \\
&= \mathbb{E}\{\sum_{m=1}^{M} |\hat{h}_{l,m,k}|^2 |e'_{l,k,mm}|^2 |w_{l,m,k}|^2\} \\
&+ \mathbb{E}\{\sum_{m=1}^{M} \sum_{n \neq m}^{M} |\hat{h}_{l,m,k}|^2 |e'_{l,k,nm}|^2 |w_{l,n,k}|^2\} \\
&+ \mathbb{E}\{\sum_{m=1}^{M} \sum_{n \neq m}^{M} \hat{h}_{l,m,k} e'_{l,k,mm} w_{l,m,k} \hat{h}_{l,n,k}^* e'^*_{l,k,nn} w_{l,n,k}^*\} \\
&+ \mathbb{E}\{\sum_{m=1}^{M} \sum_{n \neq m}^{M} \hat{h}_{l,n,k} e'_{l,k,nm} w_{l,m,k} \hat{h}_{l,m,k}^* e'^*_{nm} w_{l,n,k}^*\}
\end{aligned} \tag{4.50}$$

Then, we approximate as

$$\begin{aligned}
\mathbb{E}\{|\hat{\mathbf{h}}_{l,k}^T\mathbf{E}'_{l,k}\mathbf{w}_{l,k}|^2\} &\approx \frac{1}{M^2}\sum_{m=1}^{M}\mathbb{E}\{|\hat{h}_{l,m,k}|^4\}|e'_{l,k,mm}|^2 \\
&+ \frac{1}{M^2}\sum_{m=1}^{M}\sum_{n\neq m}^{M}\mathbb{E}\{|\hat{h}_{l,m,k}|^2\}\mathbb{E}\{|\hat{h}_{l,n,k}|^2\}|e'_{l,k,nm}|^2 \\
&+ \frac{1}{M^2}\sum_{m=1}^{M}\sum_{n\neq m}^{M}\mathbb{E}\{|\hat{h}_{l,m,k}|^2\}\mathbb{E}\{|\hat{h}_{l,n,k}|^2\}e'_{l,k,mm}e^{'*}_{l,k,nn} \\
&= \frac{2}{M^2}\sum_{m=1}^{M}|e'_{l,k,mm}|^2 + \frac{1}{M^2}\sum_{m=1}^{M}\sum_{n\neq m}^{M}|e'_{l,k,nm}|^2 + \frac{1}{M^2}\sum_{m=1}^{M}\sum_{n\neq m}^{M}e'_{l,k,mm}e^{'*}_{l,k,nn} \\
&= \frac{2}{M^2}\sum_{m=1}^{M}|e'_{l,k,mm}|^2 + \frac{1}{M^2}\sum_{m=1}^{M}\sum_{n\neq m}^{M}|e'_{l,k,nm}|^2 \\
&+ \frac{1}{M^2}\left(|\sum_{m=1}^{M}e'_{l,k,mm}|^2 - \sum_{m=1}^{M}|e'_{l,k,mm}|^2\right) \\
&= \frac{1}{M^2}\left(\mathsf{tr}(\mathbf{E}^{'\dagger}_{l,k}\mathbf{E}'_{l,k}) + |\mathsf{tr}(\mathbf{E}'_{l,k})|^2\right)
\end{aligned} \tag{4.51}$$

Next, we consider the power of the intended signal for the k'th user that is received at the kth user

$$\begin{aligned}
\mathbb{E}\{|\hat{\mathbf{h}}_{l,k}^T\mathbf{E}'_{l,k}\mathbf{w}_{l,k'}|^2\} &= \mathbb{E}\{|\sum_{m=1}^{M}\sum_{n=1}^{M}\hat{h}_{l,m,k}e'_{l,k,mn}w_{l,n,k'}|^2\} \\
&= \mathbb{E}\{\sum_{m=1}^{M}\sum_{n=1}^{M}\sum_{m'=1}^{M}\sum_{n'=1}^{M}\hat{h}_{l,m,k}e'_{l,k,mn}w_{l,n,k'}\hat{h}^*_{l,m',k}e^{'*}_{l,k,m'n'}w^*_{l,n',k'}\} \\
&= \mathbb{E}\{\sum_{m=1}^{M}|\hat{h}_{l,m,k}|^2|e'_{l,k,mm}|^2|w_{l,m,k'}|^2\} \\
&+ \mathbb{E}\{\sum_{m=1}^{M}\sum_{n\neq m}^{M}|\hat{h}_{l,m,k}|^2|e'_{l,k,nm}|^2|w_{l,n,k'}|^2\} \\
&+ \mathbb{E}\{\sum_{m=1}^{M}\sum_{n\neq m}^{M}\hat{h}_{l,m,k}e'_{l,k,mm}w_{l,m,k'}\hat{h}^*_{l,n,k}e^{'*}_{l,k,nn}w^*_{l,n,k'}\} \\
&+ \mathbb{E}\{\sum_{m=1}^{M}\sum_{n\neq m}^{M}\hat{h}_{l,n,k}e'_{l,k,nm}w_{l,m,k'}\hat{h}^*_{l,m,k}e^{'*}_{nm}w^*_{l,n,k'}\}
\end{aligned} \tag{4.52}$$

Then, we approximate as

$$\begin{aligned}\mathbb{E}\{|\hat{\mathbf{h}}_{l,k}^T\mathbf{E}'_{l,k}\mathbf{w}_{l,k'}|^2\}&\\ &\approx \sum_{m=1}^{M}\mathbb{E}\{|\hat{h}_{l,m,k}|^2\}\mathbb{E}\{|w_{l,m,k'}|^2\}|e'_{l,k,mm}|^2\\ &+\sum_{m=1}^{M}\sum_{n\neq m}^{M}\mathbb{E}\{|\hat{h}_{l,m,k}|^2\}\mathbb{E}\{|w_{l,n,k'}|^2\}|e'_{l,k,nm}|^2\\ &+\sum_{m=1}^{M}\sum_{n\neq m}^{M}\underbrace{\mathbb{E}\{\hat{h}_{l,m,k}w_{l,m,k'}\hat{h}^*_{l,n,k}w^*_{l,n,k'}\}}_{T1}e'_{l,k,mm}e'^*_{l,k,nn}\end{aligned} \tag{4.53}$$

In the absence of non-reciprocity, the inter-user interference $\mathbb{E}\{|\hat{\mathbf{h}}_{l,k}^T\mathbf{w}_{l,k'}|^2\}$ is zero, hence we approximate $T1$ based on that as follows

$$\frac{1}{M-K}+T1\cdot M(M-1)=0 \implies T1=-\frac{1}{M(M-1)(M-K)} \tag{4.54}$$

We introduce $T1$ in $\mathbb{E}\{|\hat{\mathbf{h}}_{l,k}^T\mathbf{E}'_{l,k}\mathbf{w}_{l,k'}|^2\}$ and then we have

$$\begin{aligned}\mathbb{E}\{|\hat{\mathbf{h}}_{l,k}^T\mathbf{E}'_{l,k}\mathbf{w}_{l,k'}|^2\}&\approx \frac{1}{M(M-K)}\sum_{m=1}^{M}|e'_{l,k,mm}|^2+\frac{1}{M(M-K)}\sum_{m=1}^{M}\sum_{n\neq m}^{M}|e'_{l,k,nm}|^2\\ &-\frac{1}{M(M-1)(M-K)}\sum_{m=1}^{M}\sum_{n\neq m}^{M}e'_{l,k,mm}e'^*_{l,k,nn}\\ &=\frac{\mathsf{tr}(\mathbf{E}'^{\dagger}_{l,k}\mathbf{E}'_{l,k})}{M(M-K)}-\frac{1}{M(M-1)(M-K)}\left(|\sum_{m=1}^{M}e'_{l,k,mm}|^2-\sum_{m=1}^{M}|e'_{l,k,mm}|^2\right)\\ &=\frac{\mathsf{tr}(\mathbf{E}'^{\dagger}_{l,k}\mathbf{E}'_{l,k})}{M(M-K)}+\frac{\mathsf{diag}(\mathbf{E}'^{\dagger}_{l,k})\cdot\mathsf{diag}(\mathbf{E}'_{l,k})}{M(M-1)(M-K)}-\frac{|\mathsf{tr}(\mathbf{E}'_{l,k})|^2}{M(M-1)(M-K)}\end{aligned} \tag{4.55}$$

The beamforming uncertainty is then given by

$$\begin{aligned}\mathbb{E}\{|\mathsf{BU}_k|^2\}&=\rho_d\mathsf{Var}\left(\sum_{l=1}^{L}\sqrt{\eta_{l,k}}\mathbf{g}_{l,k}^T\mathbf{w}_{l,k}\right)=\rho_d\sum_{l=1}^{L}\eta_{l,k}\mathsf{Var}(\mathbf{g}_{l,k}^T\mathbf{w}_{l,k})\\ &=\rho_d\sum_{l=1}^{L}\eta_{l,k}\frac{\mathsf{tr}(\mathbf{E}'^{\dagger}_{l,k}\mathbf{E}'_{l,k})}{M^2}+\rho_d\sum_{l=1}^{L}\eta_{l,k}\frac{(\beta_{l,k}-\phi_{l,k})}{\phi_{l,k}M(M-K)}\mathsf{tr}(\mathbf{E}^{\dagger}_{l,k}\mathbf{E}_{l,k})\end{aligned} \tag{4.56}$$

The inter-user interference yields

$$\begin{aligned}\mathbb{E}\{|\mathsf{IUI}_{k,k'}|^2\} &= \rho_d \mathbb{E}\{|\sum_{l=1}^{L} \eta_{l,k} \mathbf{g}_{l,k}^T \mathbf{w}_{l,k'}|^2\} \\ &= \rho_d \sum_{l=1}^{L} \eta_{l,k} \mathbb{E}\{|\mathbf{g}_{l,k}^T \mathbf{w}_{l,k'}|^2\} \\ &= \rho_d \sum_{l=1}^{L} \eta_{l,k} (\mathbb{E}\{|\hat{\mathbf{h}}_{l,k}^T \mathbf{E}'_{l,k} \mathbf{w}_{l,k'}|^2\} + \mathbb{E}\{|\tilde{\mathbf{h}}_{l,k}^T \mathbf{E}_{l,k} \mathbf{w}_{l,k'}|^2\}) \\ &= \rho_d \sum_{l=1}^{L} \eta_{l,k} \left(\frac{\mathsf{tr}(\mathbf{E}_{l,k}^{'\dagger} \mathbf{E}'_{l,k})}{M(M-K)} + \frac{\mathsf{diag}(\mathbf{E}_{l,k}^{'\dagger}) \cdot \mathsf{diag}(\mathbf{E}'_{l,k})}{M(M-1)(M-K)} \right. \\ &\left. - \frac{|\mathsf{tr}(\mathbf{E}'_{l,k})|^2}{M(M-1)(M-K)} \right) + \rho_d \sum_{l=1}^{L} \eta_{l,k} \frac{(\beta_{l,k} - \phi_{l,k})}{\phi_{l,k'} M(M-K)} \mathsf{tr}(\mathbf{E}_{l,k}^{\dagger} \mathbf{E}_{l,k})\end{aligned} \tag{4.57}$$

4.2.3 Analytical discussion

Here, we emphasise on the particular case of single-antenna Cell-Free massive MIMO with maximum-ratio transmission because this is the most common Cell-Free Massive MIMO scenario.

We also consider the particular case of perfect channel estimation at the AP side with maximum-ratio transmission and fixed-power-per-AP power control scheme. We aim to simplify the general analytical expressions and to obtain insight on the effects of the NRC alone.

There is only one antenna element at each AP and the uplink channel estimate power at the lth AP is now $\phi_{l,k} = \Delta_{l,k}^{\mathsf{ul}}$, while the desired signal power or the beamforming gain and the self-interference plus inter-user interference power are given by

$$\mathsf{E}\{|\mathsf{DS}_k|^2\} = |a_k|^2 |b_k|^2 \left| \sum_{l=1}^{L} \eta_{l,k}^{1/2} \frac{|R_l|^2}{R_l} \beta_{mk} T_l \right|^2 \tag{4.58}$$

$$\mathsf{E}\left\{|\mathsf{BU}_k|^2\right\} + \mathsf{E}\left\{|\mathsf{IUI}_k|^2\right\} = \sum_{m=1}^{M} |b_k|^2 |T_l|^2 \beta_{l,k} \sum_{k'=1}^{K} \eta_{l,k'} |a_{k'}|^2 |R_l|^2 \beta_{l,k'} \tag{4.59}$$

Impact of UE non-reciprocity

Based on (4.58) and (4.59), we observe that only the UE amplitude response appears; hence, the UE phase response does not explicitly impact the expressions. The interference terms in (4.59) only contain the product of the uplink and downlink transceiver frequency responses; thus, a non-reciprocal response at UE side does not affect the

interference power. Furthermore, in (4.58), the product of both uplink and downlink amplitude responses are present, implying that a non-reciprocal response does not reduce the beamforming gain.

Impact of AP non-reciprocity

From (4.58), we observe that the amplitude mismatch at the AP side does not reduce the beamforming gain since the uplink frequency response at the AP, R_l, is effectively normalised in amplitude.

However, based on (4.58), the phase non-reciprocity errors at APs will impact the beamforming direction, i.e. the transmitted signals from each AP to the kth user do not add up purely coherently anymore, reducing the beamforming gain. Respecting the impact on the inter-user interference in (4.59), we only observe the product of the uplink and downlink transceiver frequency responses. Hence, a non-reciprocal response does not increase the inter-user interference power.

Based on the analytical discussion, we conclude that

- UE non-reciprocity does not degrade the performance;
- AP amplitude non-reciprocity does not degrade the performance;
- AP phase non-reciprocity degrades the performance because the simultaneous transmit signals do not add up coherently at the receiver

These conclusions are valid under the assumption of MRT beamforming at APs, which is the most common assumption in Cell-Free Massive MIMO systems [30, 31, 34]. We survey the effects of NRC under Zero-Forcing precoding with numerical results in chapter 5. Additionally, we contrast the analytical conclusion with the numerical-based conclusions in chapter 5.

4.2.4 Downlink power control

Throughout this work, we consider two different power control schemes:

- **Fixed power per AP:** A fixed transmit power $\bar{\rho}_d$ is allocated to each AP, with this scheme all the users served by a certain AP have the same power control coefficient. The AP does not require information from others APs to compute the coefficients.
- **Fixed power per user:** A fixed transmit power $\bar{\rho}_d$ is allocated to each user, that implies an exchange of information between the APs since all the channel estimate powers are required to compute the power control coefficients. The overhead is not expected to be high due to the large-scale terms vary slowly in time with respect to

the propagation channel, with this scheme all the APs have the same power control coefficient for each user.

Fixed power per AP

Fixing the transmit power per AP leads to a power constraint at the lth AP given by

$$\mathbb{E}\{||\mathbf{x}_l||^2\} = \sum_{k=1}^{K} \eta_{l,k} \mathbb{E}\{||\mathbf{w}_{l,k}||^2\} = 1 \tag{4.60}$$

Assuming that the power control coefficient is the same to all the served users at the lth AP, the power control coefficients read

$$\eta_{l,k} = \frac{1}{\sum_{k=1}^{K} \mathbb{E}\{||\mathbf{w}_{l,k}||^2\}}, \quad l = 1, ..., L \tag{4.61}$$

Fixed power per user

Fixing the transmit power per user leads to a power constraint for the kth user given by

$$\sum_{l=1}^{L} \eta_{l,k} \mathbb{E}\{||\mathbf{w}_{l,k}||^2\} = 1 \tag{4.62}$$

Assuming the same power control for all AP serving the kth users, the power control coefficients yield

$$\eta_{l,k} = \frac{1}{\sum_{l=1}^{L} \mathbb{E}\{||\mathbf{w}_{l,k}||^2\}}, \quad k = 1, ..., K \tag{4.63}$$

4.3 Deployment scenario

We analyse a scenario with a total area A, where L APs and K users are uniformly and independently distributed over the cell area. Each AP is equipped with M antennas as described in previous sections.

In order to prevent boundary effects and imitate a realistic deployment scenario, the coverage area considered is an hexagon with six neighbours. In the Figure 4.2, it is shown an example of how the APs and UEs are random and uniformly distributed over the covered area.

At each cell realisation, the distances between the users and the access points are used to calculate the large-scale coefficients. The model used to calculate the large-scale coefficients is described below.

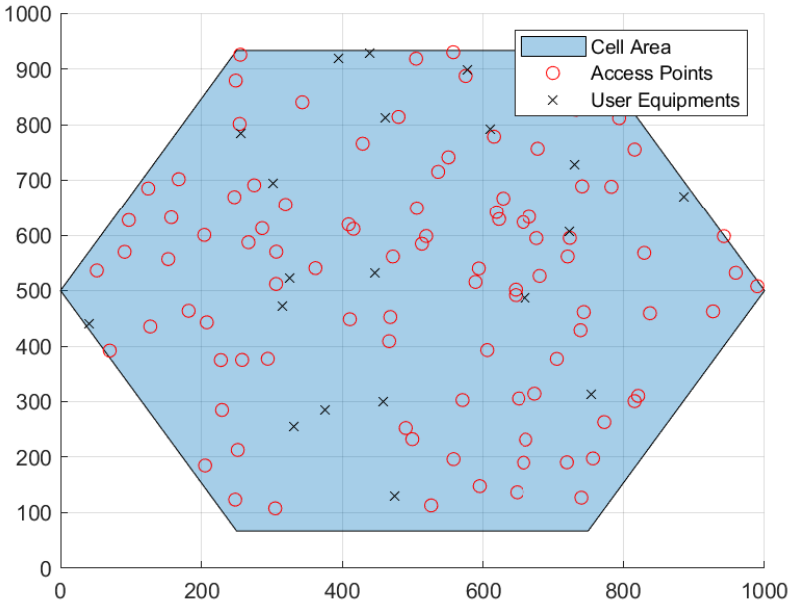

Figure 4.2. *Example of random positions of APs and UEs for* $A = 1 \times 1 km^2$ *,* $M = N = 100$ *and* $K = 20$*.*

4.3.1 Large-scale fading model

We describe the path loss and shadow fading models separately, the large-scale fading coefficient, $\beta_{l,k}$, includes both path loss and shadow fading following a log-normal distribution given by

$$\beta_{l,k} = \begin{cases} l(d_{l,k}) 10^{\frac{\sigma_{sh} z_{l,k}}{10}}, & \text{if } d_{l,k} > d_1 \\ l(d_{l,k}), & \text{if } d_1 \geq d_{l,k} \end{cases}$$

where $l(d_{l,k})$ is the path loss, $d_{l,k}$ is the distance between the lth AP and the kth user, $10^{\frac{\sigma_{sh} z_{l,k}}{10}}$ is the log-normal shadow fading with standard deviation σ_{sh} and $z_{l,k} \backsim \mathcal{N}(0,1)$. Note that there is no shadowing when the user is extremely close to the AP, i.e. when $d_1 \geq d_{l,k}$.

Multi-slope pathloss model

The model used to compute the path loss is a multi-slope model, that is the exponent increases with the propagation distance. We define two radius based on d_0 and d_1 from each AP, when the distance is larger than d_1 the exponent applied is -3.5 and when the distance is between d_0 and d_1 the exponent applied is -2.

Similar to [31], we consider the following model based on Hata-COST231 propagation model

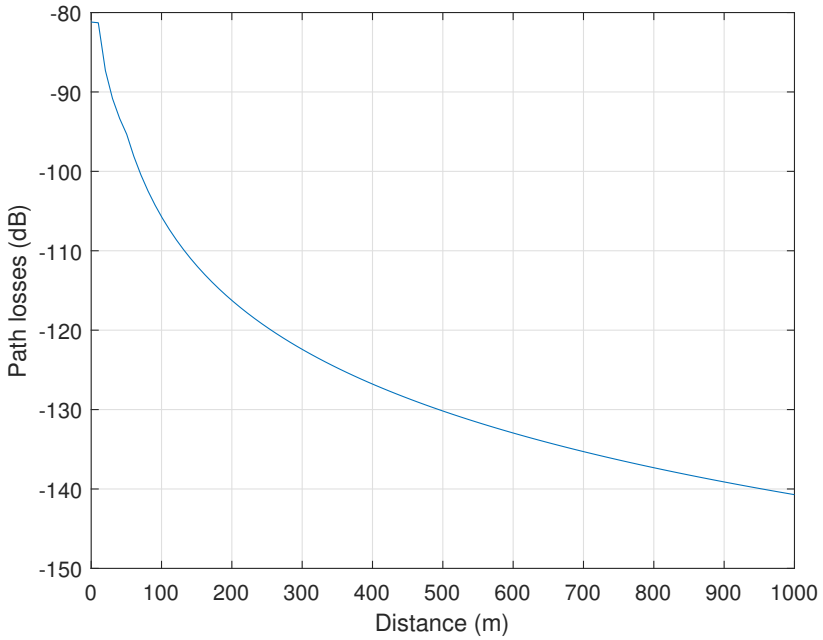

Figure 4.3. *Path losses as function of the distance.*

$$l(d_{l,k}) = \begin{cases} -L - 35\ \log_{10}(d_{l,k}), & \text{if } d_{l,k} > d_1 \\ -L - 20\ \log_{10}(d_{l,k}) - 15\ \log_{10}(d_1), & \text{if } d_1 \geq d_{l,k} > d_0 \\ -L - 20\ \log_{10}(d_0) - 15\ \log_{10}(d_1), & \text{if } d_0 \geq d_{l,k} \end{cases}$$

where L depends on the remain parameters apart from distance given by

$$\begin{aligned} L =& 46.3 + 33.9\ \log_{10}(f) - 13.82\ \log_{10}(h_{AP}) \\ & - (1.1\ \log_{10}(f) - 0.7)h_u + (1.56\ \log_{10}(f) - 0.8) \end{aligned} \tag{4.64}$$

where f is the carrier frequency, h_{AP} and h_u are the AP and user height, respectively.

In the Figure 4.4, we generate 200 realizations of 100 single-antenna APs serving 20 users and we compute the PDF of the large-scale coefficients. One can notice that the probability of being in the last slope is much higher, since the cell area is quite large the probabilty of $d_{l,k} < d_1$ is very low.

4.3.2 Deployment parameters

The principal parameters are summarised in Table 4.1, there are some considerations to take into account about some relevant calculations.

The signal-to-noise-ratio scaling coefficient can be computed by dividing the transmit

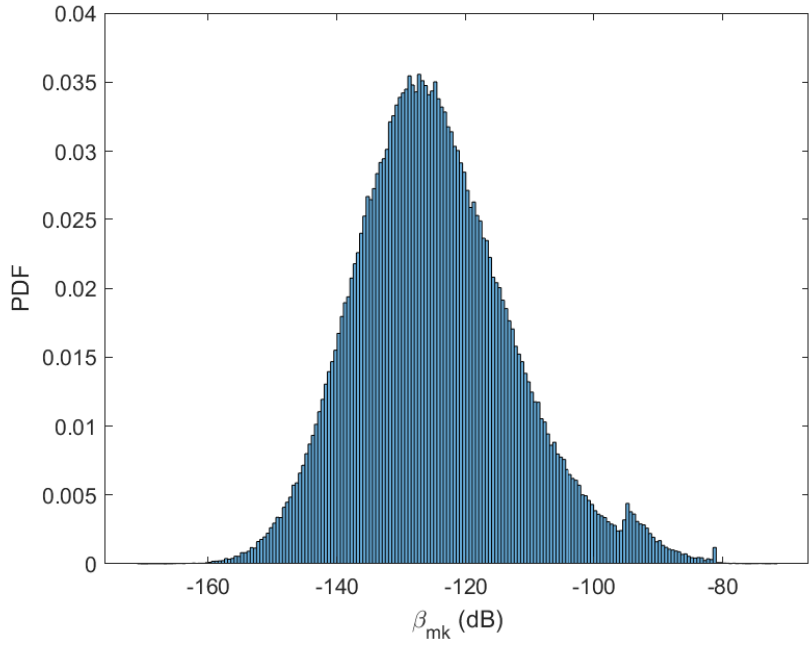

Figure 4.4. *Probability distribution function of the large-scale coefficients with multi-slope model.*

Table 4.1. *System parameters*

Parameter	Value
Number of APs: L	Varying
Number of Antennas per AP: M	Varying
Number of users: K	20
Pilot length: τ_p	20
Centre frequency: f	1.9 GHz
Antenna heights: h_{AP}, h_u	15 m, 1.65 m
Bandwidth: BW	20 MHz
Transmit powers: $\bar{\rho}_d$, $\bar{\rho}_u$	Varying
Three-slope distances: d_1, d_0	50 m, 10 m
Shadow fading deviation: σ_{sh}	8 dB
Coherence time	1 ms
Coherence bandwidth	200 kHz
Noise figure: NF	9 dB

power by the noise power, where the noise power is calculated as

$$P_N = \text{BW} \times k_B \times T_0 \times \text{NF}(W) \tag{4.65}$$

where BW is the transmission bandwidth, NF is the noise figure of the system, $k_B = 1.381 \times 10^{-23}$ is the Boltzmann constant, and $T_0 = 290K$ is the noise temperature. Hence the transmit SNR constant yields

$$\rho_x = \frac{\bar{\rho_x}}{P_N} \tag{4.66}$$

where $x \in [d, u]$.

In this work, we consider a coherence time of 1 ms and a coherence bandwidth of 200 kHz, corresponding to a coherence interval of 200 samples.

In order to compute the per-user thoughput, we consider the overhead due to channel estimation, hence the per-user throughput is given by [31]

$$S_k = BW \frac{(1 - \tau_u/\tau)}{2} R_k \tag{4.67}$$

where τ_u is the samples for the uplink training and τ is the coherence interval. This scaling factor reflects that for each coherence interval, we spend τ_u samples for the uplink training and $\tau - \tau_u$ samples for the downlink data transmission.

For the per-user spectral efficiency the process is similar, the overhead due to the uplink training has to be taken into account and the SE yields

$$R'_k = (1 - \frac{\tau_u}{\tau}) R_k \tag{4.68}$$

4.3.3 Cell-Free systems considerations

Cell-Free benefits

The main advantage of Cell-Free Massive MIMO is the macro-diversity, i.e. the distance between each user and its nearest AP is much smaller than in a centralised scenario [34]. This advantage can be noticed by using the distribution of the squared norm of the channel vector [12] also known as channel gain $||\mathbf{g}_k||^2$, this is, in fact, the gain when using maximum ratio transmission precoding.

In the Figure 4.5, we compare the channel gain $||\mathbf{g}_k||^2$ between a Cell-Free deployment with single-antenna APs and a centralised Massive MIMO system, for that we generate 200 realisations of APs and UEs locations and physical channels. The instantaneous channel gain is increased due to the spatial diversity of the Cell-Free conditions. Hence the expected achievable rate is higher in CF systems than centralised Massive MIMO systems.

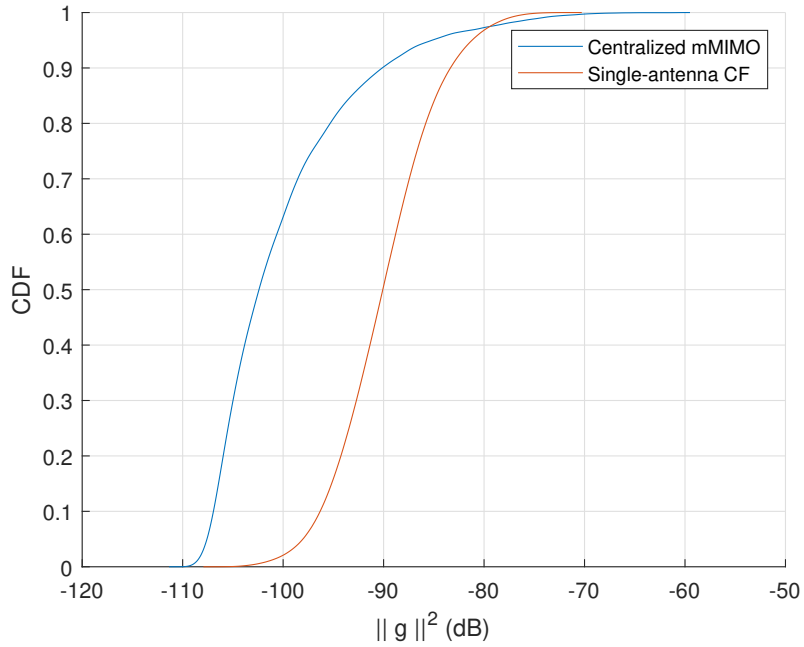

Figure 4.5. *The CDF of the channel gain. Here,* $LM = 100$ *and* $K = 20$.

Channel hardening

In classical Massive MIMO systems, the instantaneous channel gain between all the APs and each user becomes deterministic as the number of antennas increases [8, 15, 25]. This property, called channel hardening, is commonly used to reduce the signal processing complexity by avoiding estimating the effective downlink channel [25]. We present a metric to measure the channel hardening by using the *Channel Hardening Degree* similar to [17], defined as the ratio between the instantaneous effective channel gain and its average value.

$$\text{ChD}_k = 1 - \frac{\text{Var}\{||\mathbf{g}_k||_F^2\}}{|\mathbb{E}\{||\mathbf{g}_k||_F^2\}|^2} \tag{4.69}$$

as closer to 1 is ChD for the kth user, the more the channel hardens.

Previous works study the performance of channel hardening in Cell-Free scenarios [11, 12], concluding that one should not rely on channel hardening and favourable propagation when computing the achievable rates in Cell-Free Massive MIMO.

For a centralised massive MIMO system with independent Rayleigh fading channels, i.e. g_{mk} are i.i.d $\mathcal{CN}(0,1)$ RVs, the ChD_k becomes $1 - 1/M$ [18]. Hence, there is channel hardening.

A comparison of the *Channel Hardening Degree* between Cell-Free and centralised Massive MIMO is presented in Figure 4.6, where we can observe that in Cell-Free systems there is a lack of channel hardening since the squared expected value of the channel gain is not close to its power, i.e. the channel gain does have a significant variance.

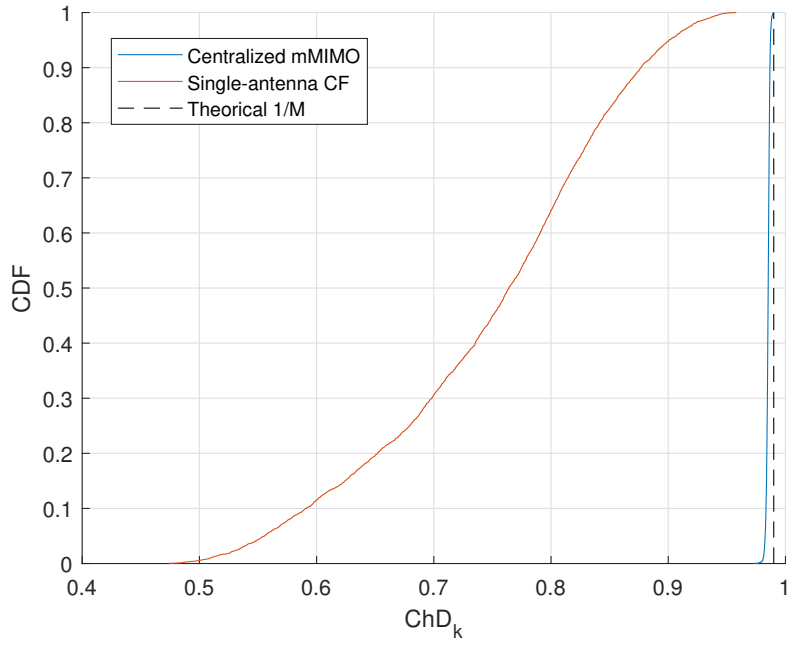

Figure 4.6. *The CDF of the Channel hardening degree. Here,* $LM = 100$ *and* $K = 20$*.*

The main implication of these results is that relying on channel hardening and favourable propagation when computing the achievable rates can lead to underestimating the real performance of the system.

Through this work, we derive analytical expressions relying on channel hardening and also considering that the users have perfect knowledge about the channel information when demodulating the received symbol, but in practical terms, it is not feasible considering that the users have that channel information as explained in chapter 2.

However, further studies are needed in terms of achievable rates in Cell-Free Massive MIMO systems, and we present conclusions based on the available rate expressions at this moment [12].

The implications of the lack of channel hardening only affect when we use the MRT precoder. In the case of ZF precoding, we need a sufficiently large number of antennas in each AP to be able to calculate the precoder matrix, and that hardens the channel [25].

A massive MIMO system employing ZF precoding produces a received scaling value at every user that is a deterministic constant. Consequently, channel statistics correspond with effective beamformed channels.

Channel hardening and non-reciprocal channels It has been shown above that Cell-Free Massive MIMO systems may, in general, suffer from a lack of channel hardening. It is also an interesting study of how a non-reciprocal response can affect channel hardening both in a centralised and a distributed case when considering fast and slow-varying non-reciprocity models presented in chapter 3.

However, in contrast to works assuming a fast-varying NRC model, the analytical results presented in this letter show that the beamforming gain uncertainty does not increase under non-reciprocal channel conditions and MRT precoding. Specifically, the gain uncertainty with a perfect channel estimate is given by

$$\text{Var}(\mathbf{w}_{l,k}^{\mathsf{T}}\mathbf{g}_k) = \sum_{l=1}^{L} \eta_{l,k}|a_k|^2|b_k|^2|R_{l,m}|^2|T_{l,m}|^2\beta_{mk}^2 \tag{4.70}$$

which does not depend on the reciprocity error ratio but on the product of the transceiver responses. Thus, since the UEs use the expected value of the beamformed channel to detect the symbol, the NRC effects are captured in that statistical moment as the non-reciprocity values are assumed to vary slowly [1, 46] compared to the variations in the physical channel.

On the contrary, in works assuming fast-varying NRC models [23, 27, 39, 40, 56, 57], the beamforming gain does not decrease under non-reciprocal channels, but the beamforming gain uncertainty increases because the NRC values are assumed to be different and random between consecutive coherence intervals. Conversely, in our system model, the beamforming gain is reduced because the slow-varying phase shifts produce a non-coherent addition of the received signals. Additionally, the variance of the beamforming gain does not increase because the NRC values are captured in the beamformed channel statistics.

5 NUMERICAL ASSESSMENT

5.1 Cell-Free systems performance under ideal conditions

In this section, we present a brief study of Cell-Free systems under ideal conditions. These simulations aim to investigate the performance and particularities of Cell-Free systems before introducing non-reciprocal channels in the analysis. In later sections, we include imperfections, and we analyse and quantify their impact.

We consider the impact of different system parameters, uplink pilot power, downlink data power and the number of antenna elements in the system. Also, we compare the performance of MRT and ZF precoders under the same conditions.

Impact of the number of antennas elements

The number of antennas located in each AP can have different effects. However, increasing the number of antenna elements per AP always improve the channel hardening [11, 12].

Maintaining the same number of total antenna elements implies that we are reducing the number of APs. Thus the favourable propagation is also reduced since geographical diversity is also reduced, i.e. the distance from a particular user to its closest AP increases.

Figure 5.1a demonstrates that increasing the number of antenna elements at each AP and maintaining the total radiating elements of the system constant produces channel hardening. To verify that statement, we observe the 95th and 5th percentiles of UatF and Genie-Aided bounds, as the number of antennas per AP increases both achievable rates are more similar to each other.

However, observing Figure 5.1b where the number of APs L is kept constant, we notice that the system does not benefit from channel hardening in this case. In this scenario, both rates benefit similarly from the increasing of antenna elements, keeping a constant gap between them.

In conclusion, increasing the number of antenna elements per AP does not always recover channel hardening. It is necessary to reduce geographical diversity to obtain a better channel hardening, but geographical diversity is one of the most attractive benefits

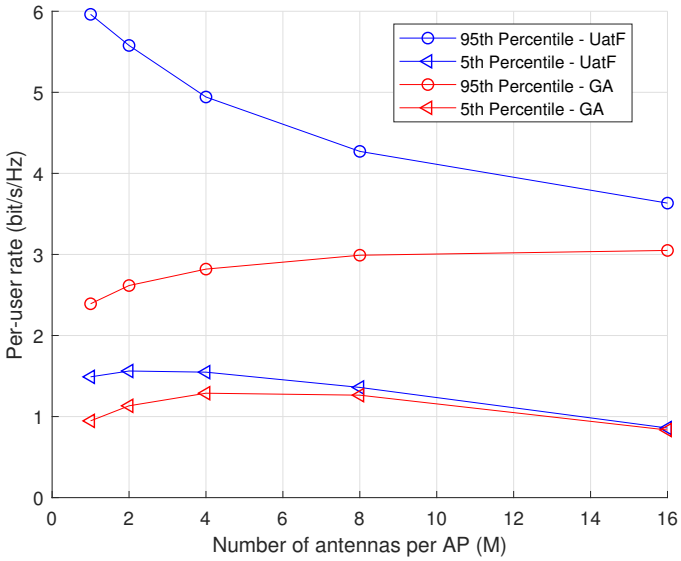

(a) $LM = 128$.

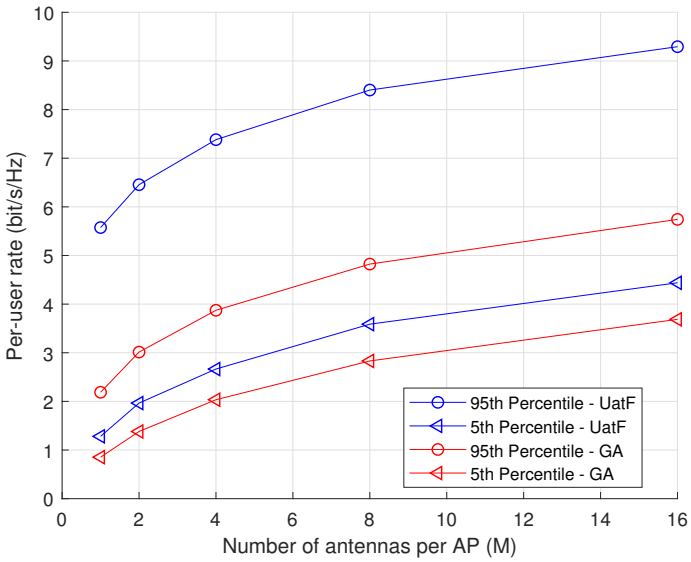

(b) $L = 100$.

Figure 5.1. *95th and 5th percentiles of the CDF of per-user rate with different antenna configurations.*

of Cell-Free systems. Thus further studies in achievable rates are needed, e.g. blind estimation, pilot optimisation.

Impact of pilot power

In this subsection, we focus on pilot power impact on the overall performance. The pilot power impacts on the quality of the uplink channel estimate, that effectively reduces the beamforming gain and increases the self-interference or beamforming gain uncertainty.

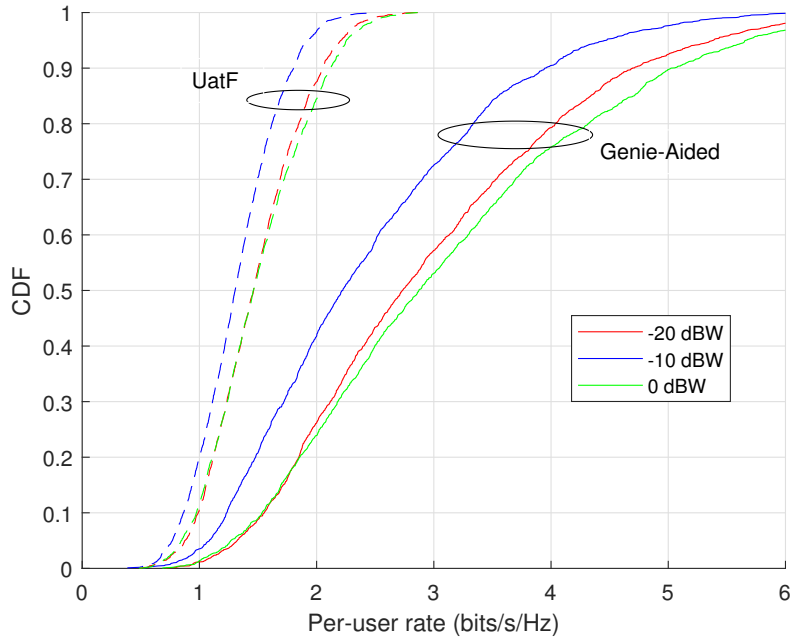

Figure 5.2. *CDF of the per-user rate under ideal conditions, different downlink powers and MRT precoder.*

The particular case of Cell-Free Massive MIMO is quite different to classic centralised Massive MIMO since the received power from each user is different in every AP, hence the received signal-to-noise ratio at each AP from each user can be different. In other words, the quality of the channel estimate differs between APs, i.e. the nearest APs to a particular user will estimate better the channel than the furthest APs.

Impact of downlink power

The allocated transmit power at the APs impacts on the received power of the desired symbol, but also in the power of the interference symbols from other users. This interference is due to the beamformed signals to the users are not orthogonal; for that reason, this interference is also called channel non-orthogonality.

Hence, increasing the transmission power does not always imply an increase in the achievable rate; there is a limit due to the interference from other users. Figure 5.2 shows the achievable rates for different per-user allocated powers, and we can observe that increasing the transmit power saturates the per-user rate.

Maximum ratio transmission vs Zero-Forcing precoder

Figure 5.3 shows the achievable rate of MRT and ZF precoders, in these simulations we choose the following system parameters: number of antenna elements per AP $M = 64$, number of APs $L = 100$ and per-user allocated power of 100 mW. We observe that ZF

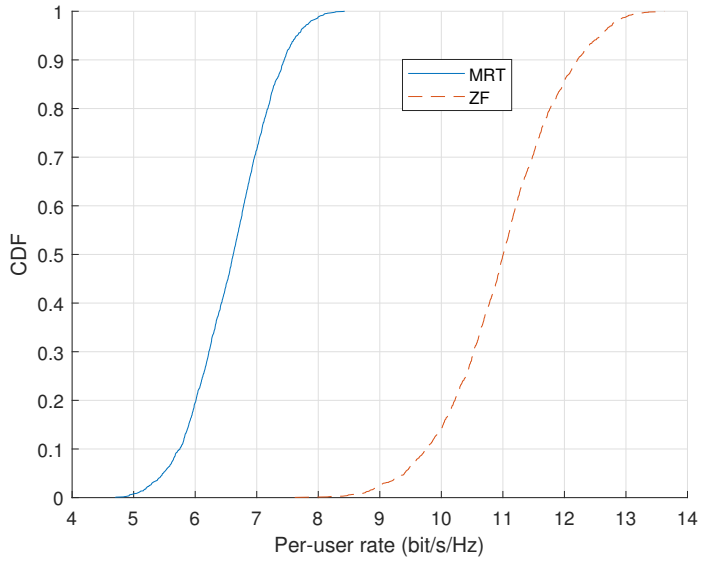

Figure 5.3. *CDF of per-user rate under MRT and ZF.* $L = 100$ *and* $M = 64$.

precoder outperforms MRT under similar ideal conditions.

5.2 Cell-Free Massive MIMO performance under non-reciprocal channels

To assess and compare the system performance under different setups and non-reciprocity levels, we use the cumulative distribution function of the per-user spectral efficiency, and in particular, the 95th and 5th percentiles. The CDF of the per-user spectral efficiency as a metric is briefly explained in chapter 2.

We generate 300 realisations, such that for each realisation, a set of UE and APs positions, generated as described in chapter 4, and the transceiver frequency response and mutual coupling matrices as described in chapter 3.

The non-reciprocity level is controlled by the parameters $\{\nu_{A_x}, \nu_{\theta_x}, \sigma^2_{MC}\}$ where $x \in [\text{AP}, \text{UE}]$. Recalling the behaviour of the model, when the system is reciprocal, i.e. both uplink and downlink responses are equal, the reciprocity level is set to $\nu = 1$.

5.2.1 Single-antenna Access Points

We take special consideration to the single-antenna APs since it is the most common approach in Cell-Free Massive MIMO systems. In this considered set up the number of antennas per AP M is set to one, and the number of APs L can vary. We only consider MRT precoding because overhead reasons, other precoders such as ZF require to exchange the CSI between APs at the channel variation rate, that requires an extensive

Parameter	Value
Number of APs: L	100
Number of antennas per AP: M	1
Number of users: K	20
Power per AP	100 mW

Table 5.1. *System parameters for single-antenna Cell-Free massive MIMO.*

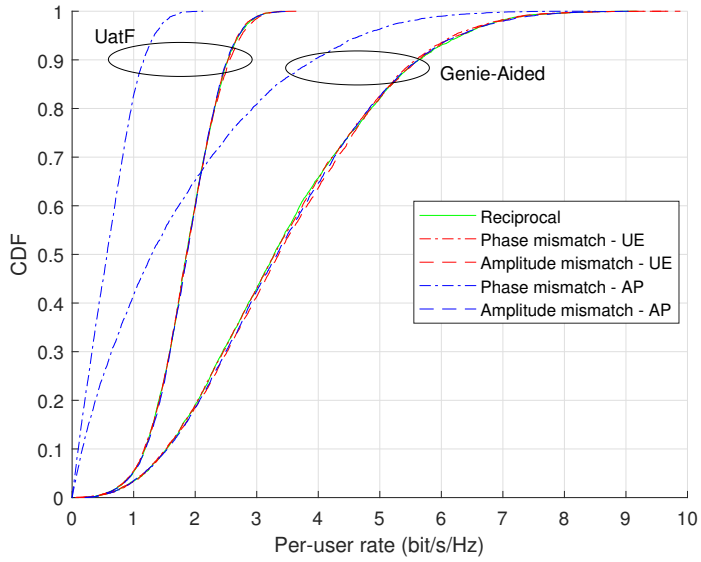

(a) *Fixed power per AP*

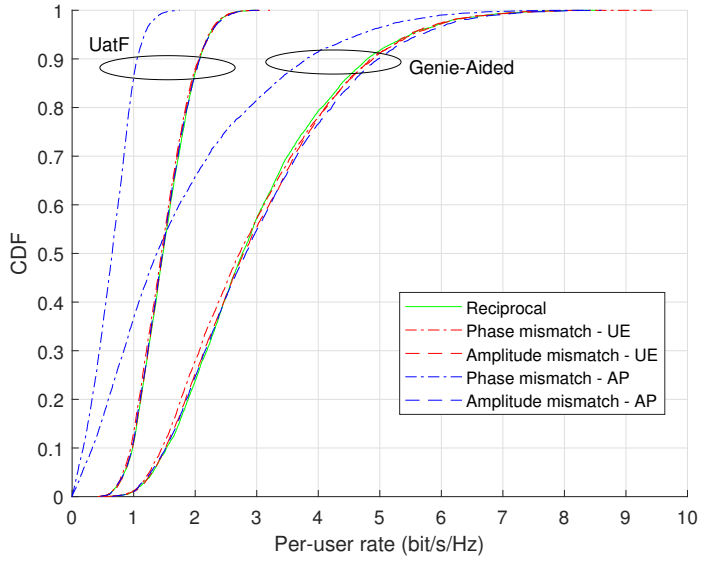

(b) *Fixed power per user*

Figure 5.4. *CDFs of MRT per-user rate under different non-reciprocity sources.* $M = 1$, $L = 100$ *and* $K = 20$. *UatF bound is blue and Genie-Aided is red.*

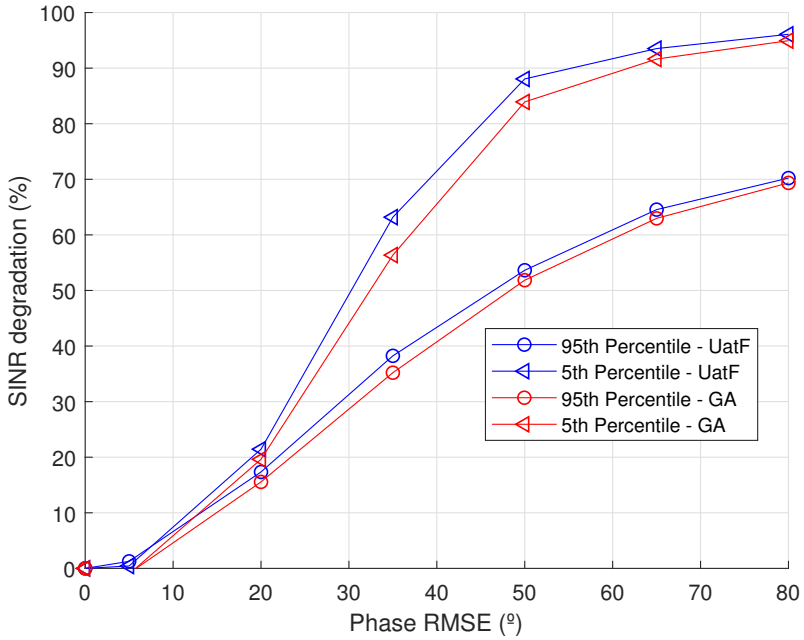

Figure 5.5. *Percentage degradation of 95th and 5th percentiles of the CDF of MRT per-user SINR under phase mismatch at APs.*

overhead in the front-haul. Hence, in single-antenna deployments, only MRT is considered in most of the works. In this Section, we choose a fixed downlink power per AP of 100 mW, and 100 mW for the uplink pilot power.

The system performance is evaluated under different non-reciprocity conditions for the following cases.

- Uplink pilot power
- Downlink data power
- Number of APs

During the analytical derivations in chapter 4, we concluded that only the phase non-reciprocity degrades the performance under these conditions. In this Section, we contrast the analytical insight with numerical conclusions.

Figure 5.4 compares the cumulative distribution function of the per-user spectral efficiency for systems under different non-reciprocity conditions. In the previous analysis, we showed that Cell-Free systems suffer from a lack of channel hardening; for that reason, we decide to present also the case in which the user knows the effective downlink channel. Here, in these simulations, the parameters of the transceiver frequency responses in uplink and downlink are uncorrelated when no reciprocity is assumed, i.e. $\nu = 0$ for each NRC case. That means that only one non-reciprocity source is considered at the same time, and the other sources are deliberately not considered. One can notice that the system performance is only sensitive to phase non-reciprocity at APs; this confirms that our previous analytical conclusions also hold for a typical uplink pilot power value.

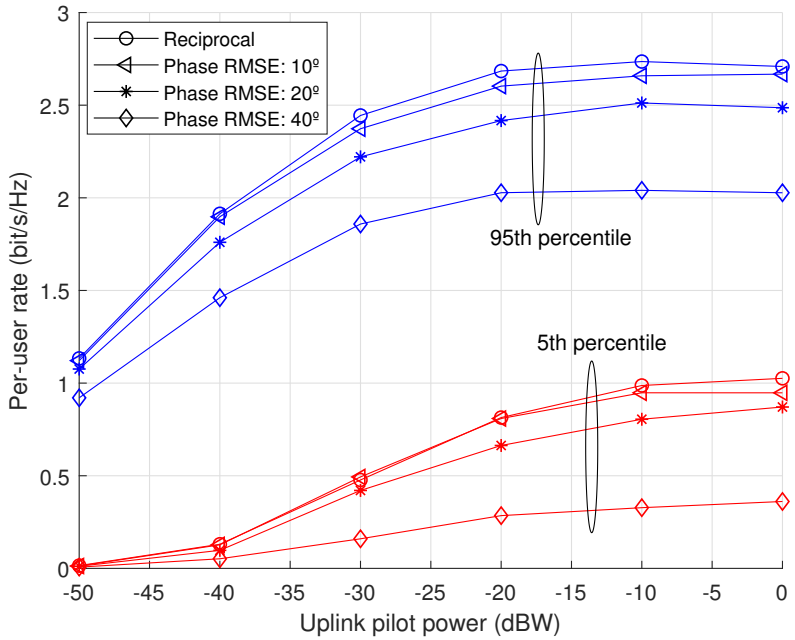

Figure 5.6. *95th and 5th percentiles of the MRT per-user UatF rate with different phase mismatches at APs and varying the number of APs.*

Furthermore, the worst case for the phase non-reciprocity at APs have a significant impact on both 95th and 5th percentiles. Furthermore, we observe that both bounds UatF and Genie-Aided are affected in the same way by different mismatches, based on that we consider the feasible UatF bound during these analyses. To verify that our analysis is independent of the power control scheme, we present the CDFs using both per-user and per-AP power control, obtaining the same conclusions from both simulations.

As we mentioned before, the fact that only phase mismatches impact performance is because the signals transmitted by the different antennas no longer add up coherently in the receiver. The transceiver amplitude and phase responses at the user do not influence the direction of the beamformed signal.

To analyse in more detail the performance degradation under phase non-reciprocity at APs Figure 5.5 shows the 5th and 95th percentiles of the per-user rate CDF for varying level of the phase non-reciprocity root mean squared error; we plot both UatF and Genie-Aided bounds.

We observe that a high-quality reciprocity calibration in terms of the AP phase errors has to be performed, specifically a non-reciprocity phase root mean squared error of 40 degrees degrades already substantially the achievable rate, particularly for the 95th percentile. This degradation highlights the importance of accurate phase reciprocity calibration at APs.

Figure 5.6 compares the degradation of 95th and 5th percentiles of the cumulative distribution function of the per-user spectral efficiency varying the number of APs. Here, we show the curves for phase non-reciprocity at APs since that is the only case that degrades

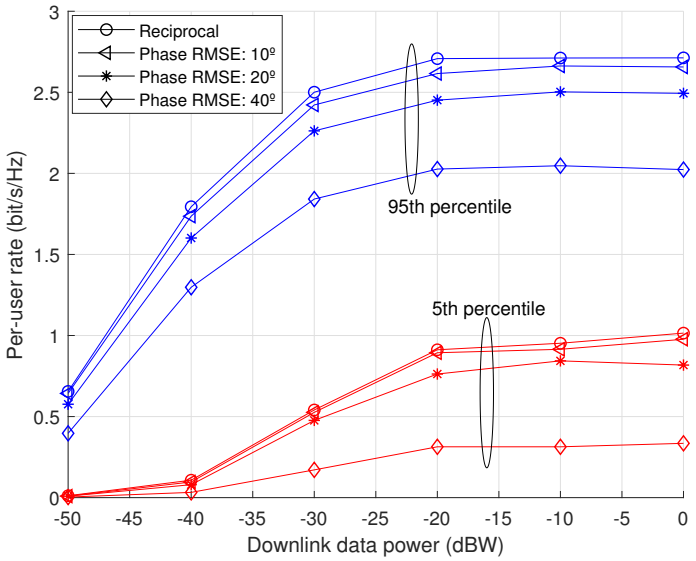

(a) *Varying the downlink data power.*

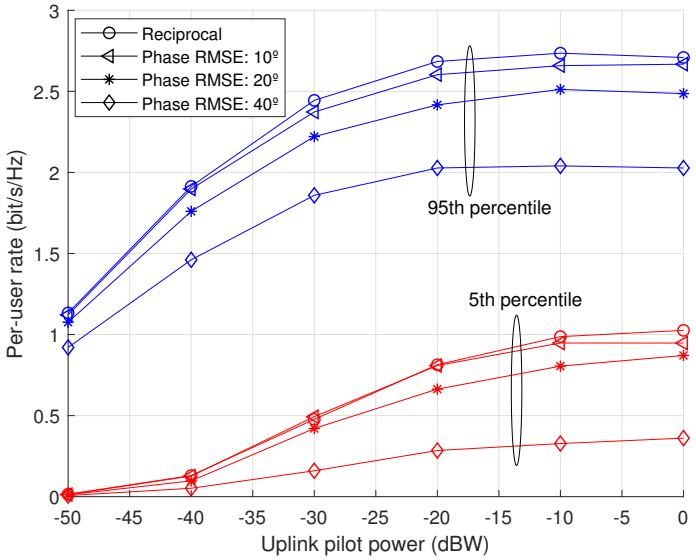

(b) *Varying the uplink pilot power.*

Figure 5.7. *95th and 5th percentiles of the MRT per-user UatF rate with different phase mismatches at APs.*

the performance, and we compare the result with the reciprocal case by expression the degradation in percentage. A critical issue raises from the results if we increase the number of antennas in the system, the per-user rate does not asymptotically converge to the reciprocal curve. Additionally, the performance under reciprocal conditions benefits from the increasing of the number of antenna elements, conversely, under non-reciprocal conditions, the achievable rate is limited by the phase mismatch and does not increase with the number of antenna elements.

To further quantify the system performance degradation, Figure 5.7b shows the SINR degradation of 95th and 5th percentiles for different uplink pilot powers. Here, we com-

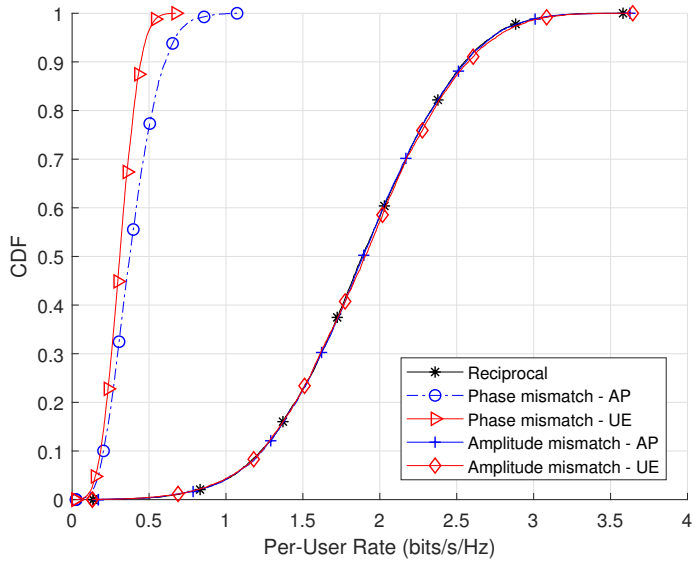

(a) *Fast-varying model.*

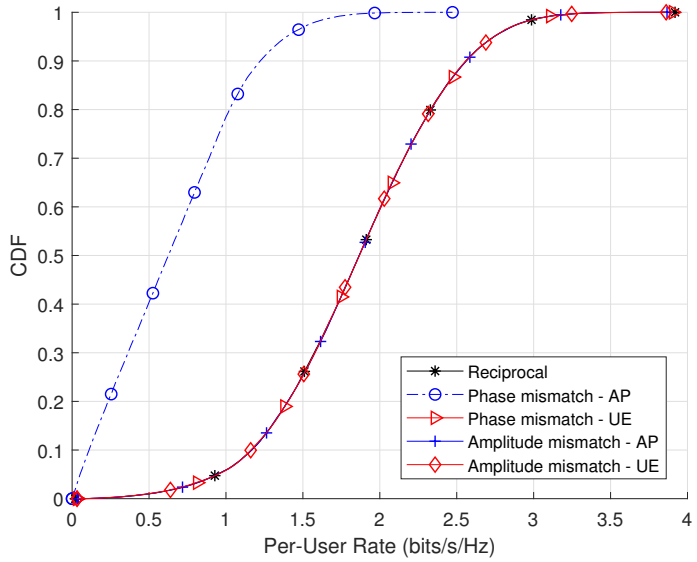

(b) *Slow-varying model.*

Figure 5.8. *CDFs of MRT with UatF per-user rate.* $L = 100$ *and* $M = 1$.

pare the reciprocal case with the non-reciprocal phase mismatch, i.e. $\nu = 0$. The ideal reciprocal case is also shown to compare the degradation that the system performance suffers from uplink pilot power. The phase non-reciprocity highly limits the per-user rate, we observe that reducing the uplink power degrades the reciprocal case, and the percentage degradation is lower than with a high uplink pilot power. The limit where the performance is no longer improved is around -20 dBW.

Fast-Varying vs Slow-Varying Non-Reciprocity Models

In chapter 3, we presented an NRC model based on physical approaches. This model includes novelty because we analytically treat the NRC parameters as unknown constants since the rate of change of NRC is much slower than the physical propagation channel.

Figures 5.8a and 5.8b compare fast and slow-varying models, in the case of Figure 5.8a, since no analytical expressions have been derived, numerical simulations are used to obtain the curves. The most remarkable difference between both models is that the fast-varying model is sensitive to UE phase non-reciprocity, whereas the slow-varying model is completely insensitive to any UE non-reciprocity. Additionally, the impact of UE non-reciprocity is greater than AP non-reciprocity, that is consistent with previous studies [40].

Many previous works do not consider UE side non-reciprocity [26, 43] because they assumed that the impact was negligible. In contrast to the fast-varying model, the slow-varying model shows analytically that UE side non-reciprocity do not affect performance. Part of the novelty of this thesis lies in this new slow-varying approach, which demonstrates that UE non-reciprocity does not affect system performance.

5.2.2 Multi-antenna Access Points

Multi-antenna Cell-Free systems promise some good advantages in terms of channel hardening or better performance with less complex deployments, hence deployments where $M > 1$ for different number of APs are considered. Obviously, if the total number of antennas increases, the system will perform better.

Maximum ratio transmission

In the first place, we analyse the impact on performance, considering MRT precoder. For that purpose, first, we survey the system performance under transceiver frequency response mismatches. Figure 5.9a investigates the degradation of the performance by increasing the number of antenna elements per AP, based on these results we demonstrate that collocating always increase the achievable rate even under practical non-reciprocal channels and we observe that the improvement ratio is the same for different phase RMSEs.

Figure 5.9b illustrates that channel also hardens under non-reciprocal channels. It shows 95th percentile of UatF and Genie-Aided bounds with different antenna configurations, as we reduce the geographical diversity, the gap between Genie-Aided and UatF also is reduced. Based on these results, we conclude that channel non-reciprocity does not worsen channel hardening.

Mutual-coupling non-reciprocity level is controlled by the variance of the mutual cou-

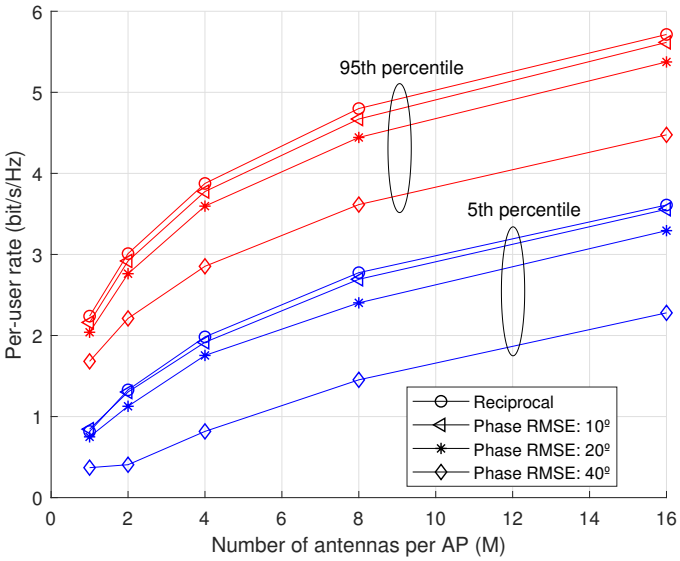

(a) *UatF bound with $L = 100$.*

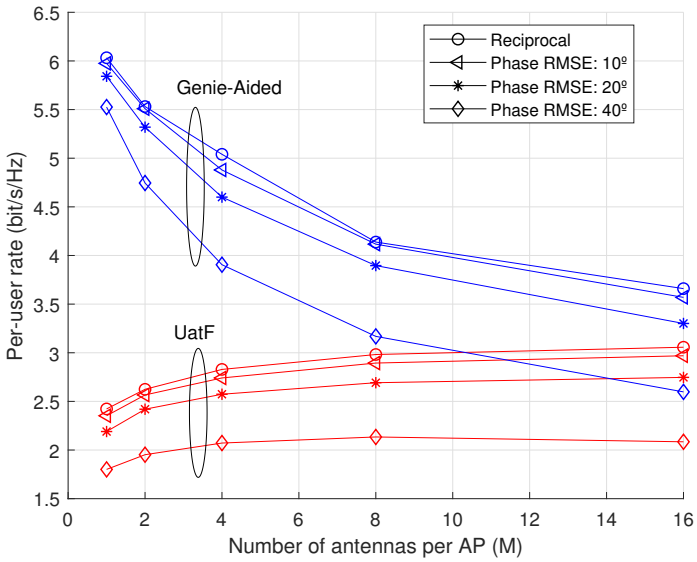

(b) *95th percentile of Genie-Aided and UatF bounds with $LM = 128$.*

Figure 5.9. *Percentiles of the CDF of MRT per-user rate with different antenna configurations and phase RMSEs.*

pling error of transmitting and receiving modes, σ^2_{MC}. Figure 5.10 demonstrates the performance of the per-user rate for MRT with different values of mutual coupling non-reciprocity variance. For this simulation, we choose a common scenario with 100 APs, 64 antennas per AP and an antenna spacing of 0.5λ. Mutual coupling non-reciprocity degrades 5th percentile substantially more than 95th; this is considerately important in order to provide a uniformly good service.

Figure 5.11 plots 95th and 5th percentiles with different number of antenna elements per AP and a mutual coupling non reciprocity variance of -15 dB. We observe that the non-reciprocal case is always clearly lower than the reciprocal and also that the degradation

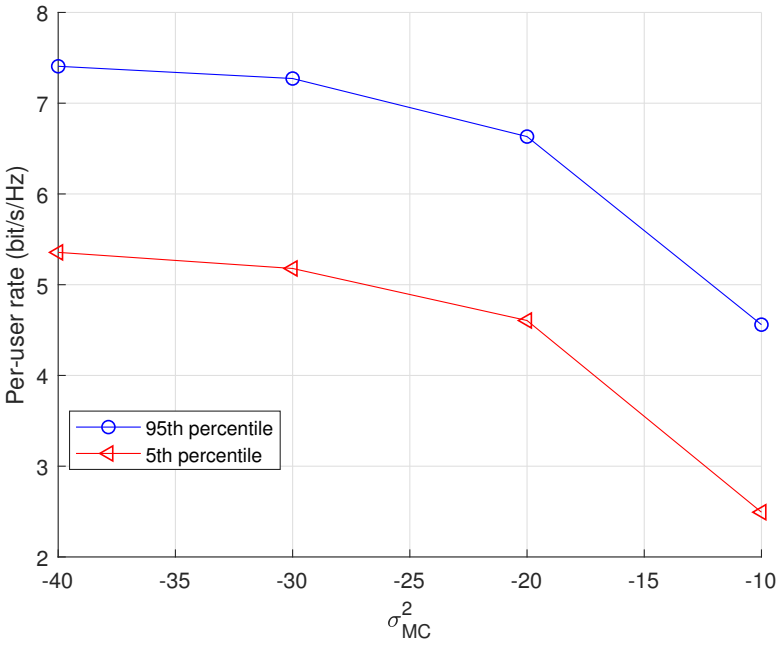

Figure 5.10. *95th and 5th percentiles of the MRT per-user UatF rate with different mutual coupling non-reciprocity variances,* $M = 64$ *and* $L = 100$*.*

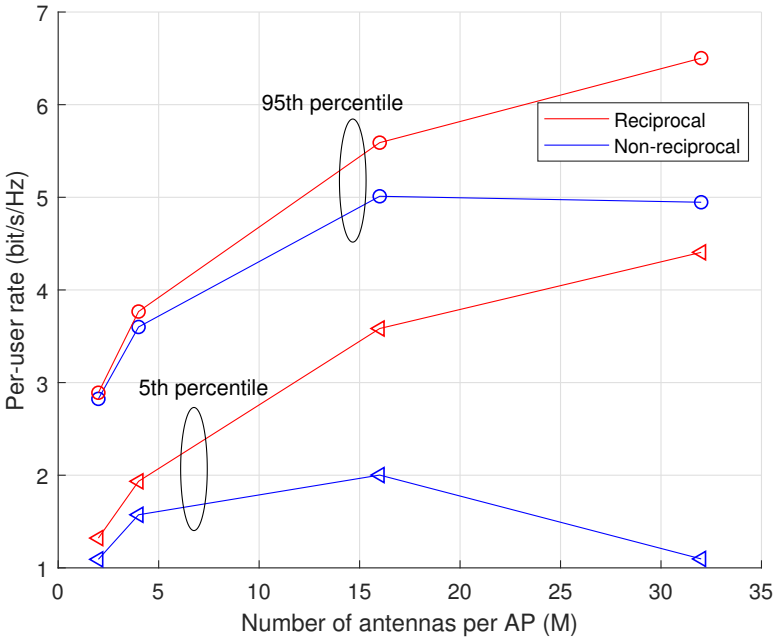

Figure 5.11. *95th and 5th percentiles of the MRT per-user UatF rate with different number of antenna elements* M*,* $L = 100$ *and* $\sigma^2_{MC} = -15$ *dB.*

Parameter	Value
Number of APs: L	100
Number of antennas per AP: M	64
Number of users: K	20
Power per user	100 mW

Table 5.2. *System parameters for ZF precoder.*

increases as the number of antennas increases. Increasing the number of antennas increases the achievable rate, but under the effect of mutual coupling non-reciprocity, the impact on performance increases as the number of antenna elements increases.

Zero-Forcing precoder

Next, we consider Zero-Forcing precoder in multi-antenna APs. The number of antennas at every AP has to be sufficiently large to allow the simultaneous transmission to the K users. In chapter 4, we present what assumptions we consider and the implications they have on system design, we presented approximations of Zero-Forcing statistical moments, and the results shown here use a proven accurate approximation.

Firstly, let us verify that the proposed approximations hold, for that purpose we set a test scenario with one AP and 100 antenna elements serving 20 users. All the users suffer the same propagation conditions controlled by the receiving SNR. Figures 5.12a, 5.12b and 5.12c verify that the approximations hold for phase, amplitude and mutual coupling mismatches.

In general, we set the following parameters; the number of users is 20, the number of antenna elements is set to 64 but can vary in simulations and the number of APs is set to 100 but can also vary during simulations. The most relevant parameters are summarised in Table 5.2.

Figure 5.13 compares in a similar way as Figure 5.4 the impact on performance of different non-reciprocity sources. There is a noticeable difference between MRT and ZF, amplitude mismatch at APs also degrades the performance and also phase error is the most degrading mismatch. In the phase non-reciprocity worst case, i.e. 104 degrees, the system performance is completely degraded. As we concluded in the MRT section, the UE non-reciprocity does not affect in any manner the system performance.

In ZF precoder case, conversely to MRT case, we analyse both phase and amplitude non-reciprocity errors. Figure 5.14a plots the percentage degradation of 95th and 5th percentiles of SINR with different phase root mean squared errors, we observe that phase errors higher than 5 - 10 degrees produce a large degradation in terms of SINR.

In the amplitude case, Figure 5.14b illustrates the SINR degradation in the same way, we observe that an amplitude root mean squared error of 0.1 produces a degradation of 30

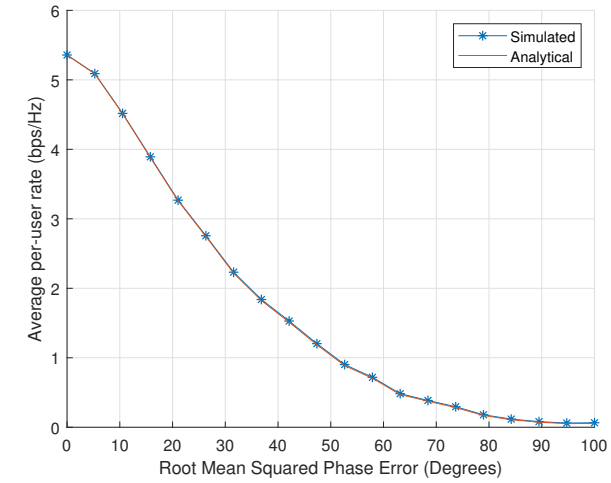

(a) *Phase mismatch*

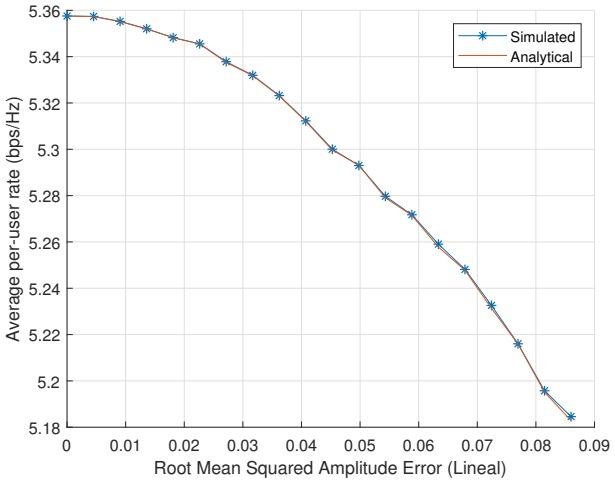

(b) *Amplitude mismatch*

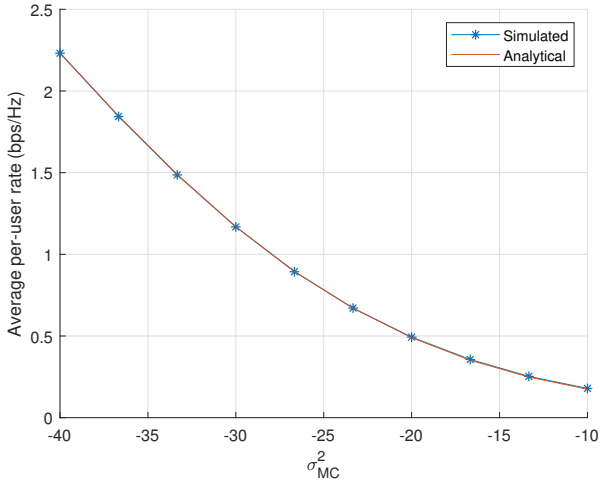

(c) *Mutual coupling mismatch*

Figure 5.12. *Average per-user rate under different mismatch sources at AP and ZF precoding with* $L = 1$, $M = 100$, $K = 20$ *and receiving SNR = 10 dB.*

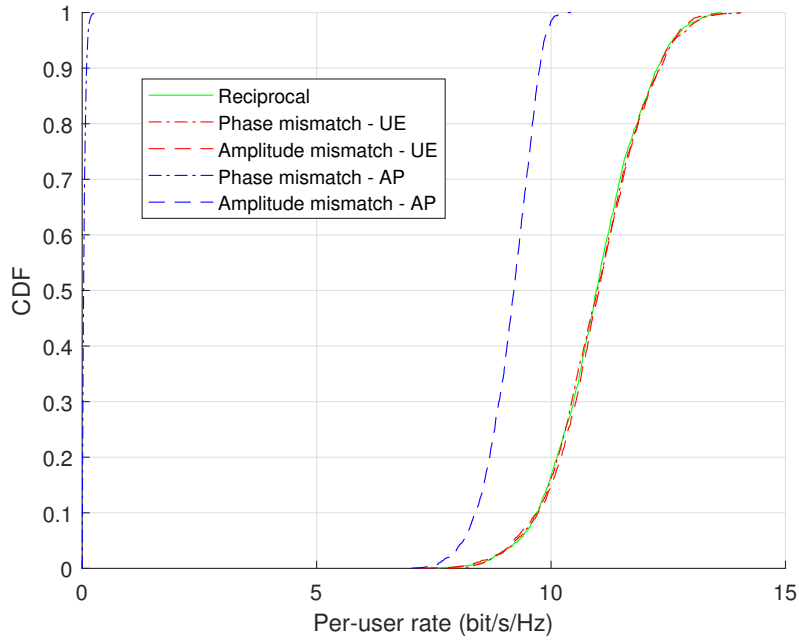

Figure 5.13. *CDFs of ZF per-user rate under different non-reciprocity sources.* $M = 64$*,* $L = 100$ *and* $K = 20$*.*

% of the 5th percentile of SINR.

Figure 5.15 shows both 95th and 5th percentiles of the ZF per-user rate with different mutual non-reciprocity variances. We observe that a variance higher than -20 dB degrades both percentiles to zero.

Figure 5.16 demonstrates that a system with a mutual coupling non-reciprocity variance of -30 dB does not benefit from an increasing of the number of antennas per AP. In this Figure, the performance of a reciprocal system is compared with the performance of a non-reciprocal system, we notice that while the reciprocal case the performance increases as the number of antennas increases, in the non-reciprocal case the performance is limited by the non-reciprocal response.

ZF and MRT comparison

Figures 5.10 and 5.15 use the same parameters to simulate the impact of mutual coupling non reciprocity, thus we can compare MRT and ZF precoders. In these Figures, we observe that Zero-Forcing precoder is far more sensitive to mutual coupling non-reciprocity than MRT precoder. A mutual coupling non-reciprocity variance of -10 dB degrades completely the performance of 5th percentile under ZF precoding, and in the case of MRT precoder, a variance of -10 dB degrades substantially the 5th percentile but to a lesser extent than ZF.

A striking difference between both precoders is that MRT is only affected by a non-reciprocal phase response, whereas ZF is affected by both amplitude and phase non-

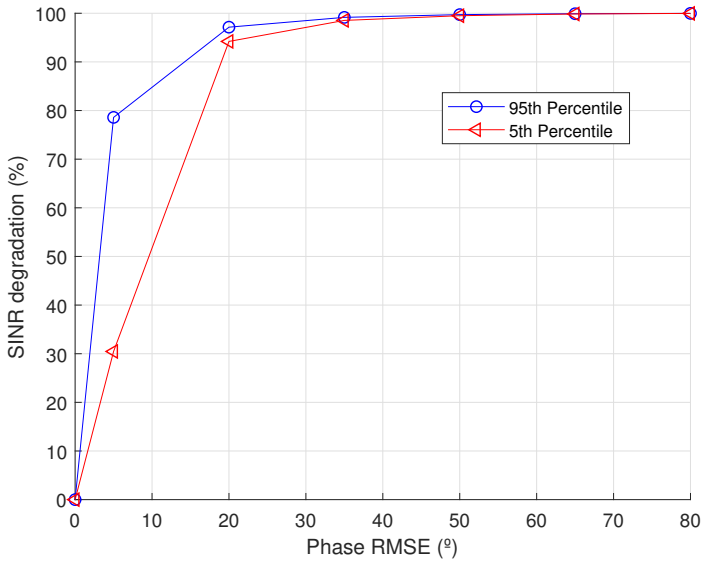

(a) *Phase mismatch*

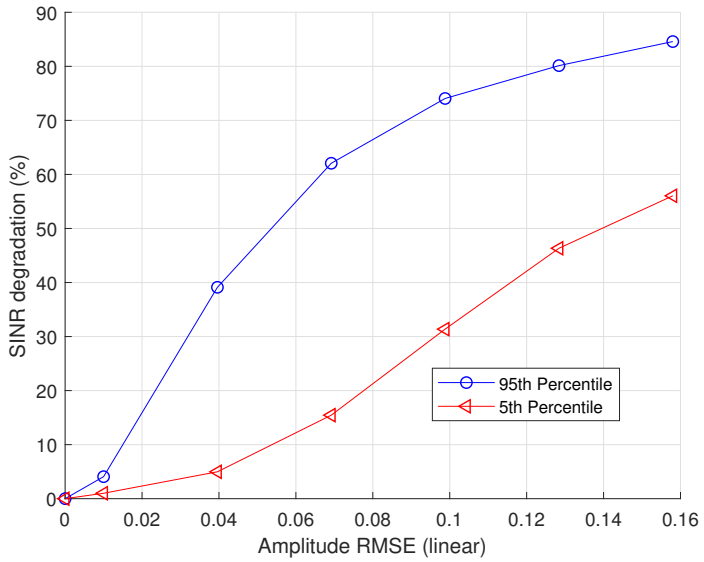

(b) *Amplitude mismatch*

Figure 5.14. *Percentage degradation of 95th and 5th percentiles of the CDF of ZF per-user SINR with* $L = 100$*,* $M = 64$ *and* $K = 20$*.*

reciprocal responses. This difference can be noticed in Figures 5.4 and 5.13, where we observe a complete degradation of both 95th and 5th percentiles in ZF case and only a complete degradation of 5th percentile in MRT case. Additionally, comparing Figures 5.5 and 5.14a, we observe that ZF is more sensitive to phase non-reciprocity than MRT. We note that 20 degrees of phase RMSE completely degrade ZF performance but MRT with UatF bound experiences the same degradation with 80 degrees of phase RMSE.

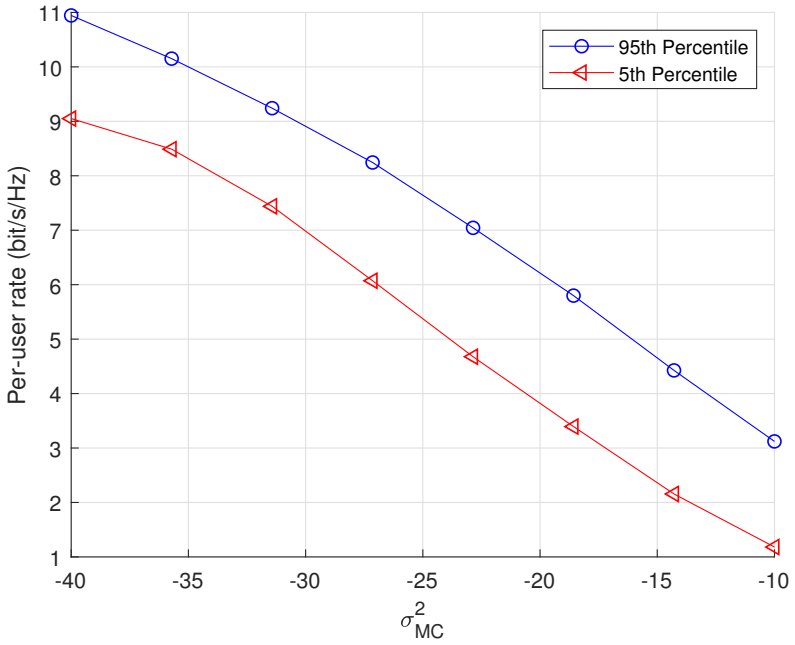

Figure 5.15. *95th and 5th percentiles of the ZF per-user rate with different mutual coupling non-reciprocity variances,* $M = 64$ *and* $L = 100$.

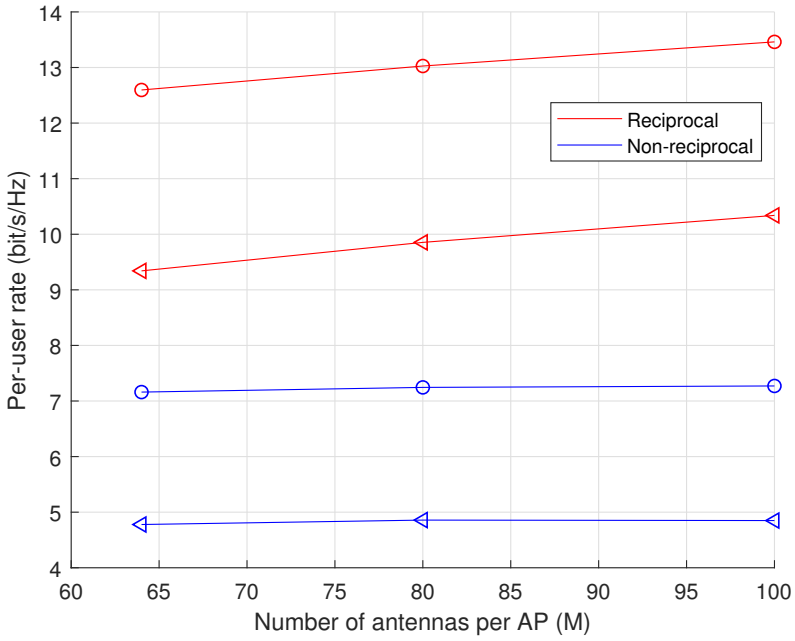

Figure 5.16. *95th and 5th percentiles of the ZF per-user rate with different number of antennas per AP* M, $\sigma^2_{MC} = -30$ *dB and* $L = 100$. *Circle and triangle represent the 95th and 5th percentiles, respectively.*

6 CONCLUSION

In this last chapter, we sum up the most relevant findings and, we also present possible future works drawn upon the scope of this thesis.

This Master's thesis aims to survey the effects of non-reciprocal channels in Cell-Free massive MIMO systems. For that purpose, we derived analytical expressions for the achievable rate using maximum ratio transmission and zero-forcing precoding, including non-reciprocal channel models. Those expressions introduce novelty because the non-reciprocity model used in this work is different from most of the previous works. Unlike previous papers, we consider a more physically-inspired model where non-reciprocity values remain constant over many coherence intervals as proved by experimental results.

Given the results from chapter 5, non-reciprocal channels can easily be a performance-limiting factor in massive MIMO systems, specifically in Cell-Free systems.

We also provide exact numerical approximations for derivations of analytical expressions using zero-forcing precoding, and we verify their consistency through numerical results.

We summarise the main findings as follows

- Non-reciprocal transceiver responses at UEs do not impact on the system performance in any manner. This conclusion contrasts with some previous works, and the reason is the slow-varying non-reciprocity model used in this work. This result entails that calibration algorithms can completely ignore the transceiver frequency response of the UEs.
- Maximum-ratio transmission is only affected by non-reciprocal phase responses at APs. Based on this finding, calibration algorithms should strongly focus on compensating phase mismatches when APs use conjugate beamforming.
- Phase non-reciprocal responses affect to a greater extent than amplitude non-reciprocal responses when APs use zero-forcing precoding. Therefore, calibration algorithms should prioritise phase than amplitude response compensation.
- Phase non-reciprocal response compensation is the most important issue in terms of system performance degradation for both conjugate beamforming and zero-forcing precoding.
- In general terms, ZF is more sensitive to all non-reciprocity sources than MRT. Mutual coupling and phase non-reciprocity have a stronger impact on ZF than MRT achievable rate.

6.1 Further studies

Further studies of this thesis should follow these guidelines.

- Exploiting calibration methods based on the conclusions of the thesis, e.g. only phase non-reciprocity errors at APs affect the MRT performance or only phase and amplitude non-reciprocity errors at APs affect the ZF performance.
- Different precoding techniques are also interesting for research purposes. Considering other precoders under non-reciprocal channels and deriving closed-form analytical expressions and conclusions is an interesting research topic for future works.
- Slow-varying non-reciprocity model can be used to analyse in an extensive way centralised massive MIMO systems, and to compare performance limitations between distributed and centralised deployments.

REFERENCES

[1] Alcatel-Lucent. *Channel Reciprocity Modeling and Performance Evaluation*. Nov. 2009.

[2] M. Alrabeiah and A. Alkhateeb. Deep Learning for TDD and FDD Massive MIMO: Mapping Channels in Space and Frequency. *arXiv:1905.03761 [cs, eess, math]* (May 2019). arXiv: 1905.03761. URL: http://arxiv.org/abs/1905.03761 (visited on 07/24/2019).

[3] M. Arnold, S. Dörner, S. Cammerer, S. Yan, J. Hoydis and S. t. Brink. Enabling FDD Massive MIMO through Deep Learning-based Channel Prediction. *arXiv:1901.03664 [cs, math, stat]* (Jan. 2019). arXiv: 1901.03664. URL: http://arxiv.org/abs/1901.03664 (visited on 07/24/2019).

[4] X. Artiga, B. Devillers and J. Perruisseau-Carrier. Mutual coupling effects in multi-user massive MIMO base stations. *Proceedings of the 2012 IEEE International Symposium on Antennas and Propagation*. July 2012, 1–2. DOI: 10.1109/APS.2012.6349354.

[5] F. Athley, G. Durisi and U. Gustavsson. Analysis of Massive MIMO with hardware impairments and different channel models. *2015 9th European Conference on Antennas and Propagation (EuCAP)*. Apr. 2015, 1–5.

[6] Balanis. *Antenna Theory: Analysis and Design, 4th Edition*. en-us. URL: https://www.wiley.com/en-us/Antenna+Theory%3A+Analysis+and+Design%2C+4th+Edition-p-9781118642061 (visited on 07/24/2019).

[7] M. E. Bialkowski, P. Uthansakul, K. Bialkowski and S. Durrani. Investigating the performance of MIMO systems from an electromagnetic perspective. en. *Microwave and Optical Technology Letters* 48.7 (2006), 1233–1238. ISSN: 1098-2760. DOI: 10.1002/mop.21664. URL: https://onlinelibrary.wiley.com/doi/abs/10.1002/mop.21664 (visited on 04/05/2019).

[8] E. Björnson, J. Hoydis and L. Sanguinetti. Massive MIMO Networks: Spectral, Energy, and Hardware Efficiency. en. *Foundations and Trends® in Signal Processing* 11.3-4 (2017), 154–655. ISSN: 1932-8346, 1932-8354. DOI: 10.1561/2000000093. URL: http://www.nowpublishers.com/article/Details/SIG-093 (visited on 05/29/2019).

[9] C. Chen, S. Blandino, A. Gaber, C. Desset, A. Bourdoux, L. V. d. Perre and S. Pollin. Distributed Massive MIMO: A Diversity Combining Method for TDD Reciprocity Calibration. *GLOBECOM 2017 - 2017 IEEE Global Communications Conference*. Dec. 2017, 1–7. DOI: 10.1109/GLOCOM.2017.8254817.

[10] X. Chen, S. Zhang and Q. Li. A Review of Mutual Coupling in MIMO Systems. *IEEE Access* 6 (2018), 24706–24719. ISSN: 2169-3536. DOI: 10.1109/ACCESS.2018.2830653.

[11] Z. Chen and E. Bjoernson. Can We Rely on Channel Hardening in Cell-Free Massive MIMO?: *2017 IEEE Globecom Workshops (GC Wkshps)*. Dec. 2017, 1–6. DOI: 10.1109/GLOCOMW.2017.8269162.

[12] Z. Chen and E. Björnson. Channel Hardening and Favorable Propagation in Cell-Free Massive MIMO With Stochastic Geometry. *IEEE Transactions on Communications* 66.11 (Nov. 2018), 5205–5219. ISSN: 0090-6778. DOI: 10.1109/TCOMM.2018.2846272.

[13] *Elements of Statistical Learning: data mining, inference, and prediction. 2nd Edition.* URL: https://web.stanford.edu/~hastie/ElemStatLearn/ (visited on 07/24/2019).

[14] O. Elijah, C. Y. Leow, T. A. Rahman, S. Nunoo and S. Z. Iliya. A Comprehensive Survey of Pilot Contamination in Massive MIMO—5G System. *IEEE Communications Surveys Tutorials* 18.2 (2016), 905–923. ISSN: 1553-877X. DOI: 10.1109/COMST.2015.2504379.

[15] S. Gunnarsson, J. Flordelis, L. Van der Perre and F. Tufvesson. Channel Hardening in Massive MIMO - A Measurement Based Analysis. *arXiv:1804.01690 [cs, math]* (Apr. 2018). arXiv: 1804.01690. URL: http://arxiv.org/abs/1804.01690 (visited on 07/24/2019).

[16] I. Gupta and A. Ksienski. Effect of mutual coupling on the performance of adaptive arrays. *IEEE Transactions on Antennas and Propagation* 31.5 (Sept. 1983), 785–791. ISSN: 0018-926X. DOI: 10.1109/TAP.1983.1143128.

[17] G. Interdonato, P. Frenger and E. G. Larsson. Utility-based Downlink Pilot Assignment in Cell-Free Massive MIMO. *WSA 2018; 22nd International ITG Workshop on Smart Antennas*. Mar. 2018, 1–8.

[18] G. Interdonato, H. Q. Ngo, E. G. Larsson and P. Frenger. How Much Do Downlink Pilots Improve Cell-Free Massive MIMO?: *2016 IEEE Global Communications Conference (GLOBECOM)*. Dec. 2016, 1–7. DOI: 10.1109/GLOCOM.2016.7841875.

[19] S. M. Kay. *Fundamentals of Statistical Signal Processing: Estimation Theory*. Upper Saddle River, NJ, USA: Prentice-Hall, Inc., 1993. ISBN: 978-0-13-345711-7.

[20] X. Liu, M. Bialkowski and F. Wang. Investigation into the Effects of Spatial Correlation on MIMO Channel Estimation and Capacity. *2008 4th International Conference on Wireless Communications, Networking and Mobile Computing*. Oct. 2008, 1–4. DOI: 10.1109/WiCom.2008.91.

[21] X. Liu and M. E. Bialkowski. *Effect of Antenna Mutual Coupling on MIMO Channel Estimation and Capacity*. en. Research article. 2010. DOI: 10.1155/2010/306173. URL: https://www.hindawi.com/journals/ijap/2010/306173/ (visited on 04/05/2019).

[22] X. Luo. How Accurate Calibration Is Needed in Massive MIMO?: *2015 IEEE Globecom Workshops (GC Wkshps)*. Dec. 2015, 1–6. DOI: 10.1109/GLOCOMW.2015.7414054.

[23] X. Luo. Multiuser Massive MIMO Performance With Calibration Errors. *IEEE Transactions on Wireless Communications* 15.7 (July 2016), 4521–4534. ISSN: 1536-1276. DOI: 10.1109/TWC.2016.2542135.

[24] T. L. Marzetta. Massive MIMO: An Introduction. *Bell Labs Technical Journal* 20 (2015), 11–22. ISSN: 1538-7305. DOI: 10.15325/BLTJ.2015.2407793.

[25] T. L. Marzetta, E. G. Larsson, H. Yang and H. Q. Ngo. *Fundamentals of Massive MIMO by Thomas L. Marzetta*. en. Nov. 2016. DOI: 10.1017/CBO9781316799895. URL: /core/books/fundamentals-of-massive-mimo/C43AF993A6DA7075EC5F186F6BAC914B (visited on 07/24/2019).

[26] D. Mi, M. Dianati, L. Zhang, S. Muhaidat and R. Tafazolli. Massive MIMO Performance With Imperfect Channel Reciprocity and Channel Estimation Error. *IEEE Transactions on Communications* 65.9 (Sept. 2017), 3734–3749. ISSN: 0090-6778. DOI: 10.1109/TCOMM.2017.2676088.

[27] A. Minasian, S. Shahbazpanahi and R. S. Adve. Distributed Massive MIMO Systems With Non-Reciprocal Channels: Impacts and Robust Beamforming. *IEEE Transactions on Communications* 66.11 (Nov. 2018), 5261–5277. ISSN: 0090-6778. DOI: 10.1109/TCOMM.2018.2859937.

[28] A. Mohammadi and F. M. Ghannouchi. *RF Transceiver Design for MIMO Wireless Communications*. en. Lecture Notes in Electrical Engineering. Berlin Heidelberg: Springer-Verlag, 2012. ISBN: 978-3-642-27634-7. URL: https://www.springer.com/gp/book/9783642276347 (visited on 07/24/2019).

[29] E. Nayebi, A. Ashikhmin, T. L. Marzetta, H. Yang and B. D. Rao. Precoding and Power Optimization in Cell-Free Massive MIMO Systems. *IEEE Transactions on Wireless Communications* 16.7 (July 2017), 4445–4459. ISSN: 1536-1276. DOI: 10.1109/TWC.2017.2698449.

[30] E. Nayebi, A. Ashikhmin, T. L. Marzetta and H. Yang. Cell-Free Massive MIMO systems. en. *2015 49th Asilomar Conference on Signals, Systems and Computers*. Pacific Grove, CA, USA: IEEE, Nov. 2015, 695–699. ISBN: 978-1-4673-8576-3. DOI: 10.1109/ACSSC.2015.7421222. URL: http://ieeexplore.ieee.org/document/7421222/ (visited on 04/18/2019).

[31] H. Q. Ngo, A. Ashikhmin, H. Yang, E. G. Larsson and T. L. Marzetta. Cell-Free Massive MIMO Versus Small Cells. *IEEE Transactions on Wireless Communications* 16.3 (Mar. 2017), 1834–1850. ISSN: 1536-1276. DOI: 10.1109/TWC.2017.2655515.

[32] H. Q. Ngo and E. G. Larsson. No Downlink Pilots Are Needed in TDD Massive MIMO. *IEEE Transactions on Wireless Communications* 16.5 (May 2017), 2921–2935. ISSN: 1536-1276. DOI: 10.1109/TWC.2017.2672540.

[33] H. Q. Ngo. *Massive MIMO: Fundamentals and System Designs*. en. Google-Books-ID: wiGKBwAAQBAJ. Linköping: Linköping University Electronic Press, Jan. 2015. ISBN: 978-91-7519-147-8.

[34] H. Q. Ngo, A. Ashikhmin, H. Yang, E. G. Larsson and T. L. Marzetta. Cell-Free Massive MIMO: Uniformly great service for everyone. en. *2015 IEEE 16th International Workshop on Signal Processing Advances in Wireless Communications (SPAWC)*.

Stockholm, Sweden: IEEE, June 2015, 201–205. ISBN: 978-1-4799-1931-4. DOI: 10.1109/SPAWC.2015.7227028. URL: http://ieeexplore.ieee.org/document/7227028/ (visited on 04/18/2019).

[35] M. Petermann, M. Stefer, F. Ludwig, D. Wubben, M. Schneider, S. Paul and K. Kammeyer. Multi-User Pre-Processing in Multi-Antenna OFDM TDD Systems with Non-Reciprocal Transceivers. *IEEE Transactions on Communications* 61.9 (Sept. 2013), 3781–3793. ISSN: 0090-6778. DOI: 10.1109/TCOMM.2013.072813.120984.

[36] J. R. Pierce. *An Introduction to Information Theory: Symbols, Signals and Noise*. English. Subsequent edition. New York: Dover Publications, Nov. 1980. ISBN: 978-0-486-24061-9.

[37] M.-O. Pun, M. Morelli and C.-C. J. Kuo. *Multi-carrier Techniques for Broadband Wireless Communications: A Signal Processing Perspective*. en. Google-Books-ID: PSRqDQAAQBAJ. World Scientific, 2007. ISBN: 978-1-86094-946-3.

[38] O. Raeesi, A. Gokceoglu, P. C. Sofotasios, M. Renfors and M. Valkama. Modeling and estimation of massive MIMO channel non-reciprocity: Sparsity-aided approach. *2017 25th European Signal Processing Conference (EUSIPCO)*. Aug. 2017, 2596–2600. DOI: 10.23919/EUSIPCO.2017.8081680.

[39] O. Raeesi, A. Gokceoglu and M. Valkama. Estimation and Mitigation of Channel Non-Reciprocity in Massive MIMO. *IEEE Transactions on Signal Processing* 66.10 (May 2018), 2711–2723. ISSN: 1053-587X. DOI: 10.1109/TSP.2018.2814992.

[40] O. Raeesi, A. Gokceoglu, Y. Zou, E. Björnson and M. Valkama. Performance Analysis of Multi-User Massive MIMO Downlink Under Channel Non-Reciprocity and Imperfect CSI. *IEEE Transactions on Communications* 66.6 (June 2018), 2456–2471. ISSN: 0090-6778. DOI: 10.1109/TCOMM.2018.2792017.

[41] O. Raeesi, Y. Zou, A. Tölli and M. Valkama. Closed-form analysis of channel non-reciprocity due to transceiver and antenna coupling mismatches in multi-user massive MIMO network. *2014 IEEE Globecom Workshops (GC Wkshps)*. Dec. 2014, 333–339. DOI: 10.1109/GLOCOMW.2014.7063453.

[42] B. Ramamurthi. Cutting edge at the cell edge: Co-channel interference mitigation in emerging broadband wireless systems. *2009 First International Communication Systems and Networks and Workshops*. Jan. 2009, 1–7. DOI: 10.1109/COMSNETS.2009.4808881.

[43] R. Rogalin, O. Y. Bursalioglu, H. C. Papadopoulos, G. Caire and A. F. Molisch. Hardware-impairment compensation for enabling distributed large-scale MIMO. *2013 Information Theory and Applications Workshop (ITA)*. Feb. 2013, 1–10. DOI: 10.1109/ITA.2013.6502966.

[44] H. Rohling, ed. *OFDM: Concepts for Future Communication Systems*. en. Signals and Communication Technology. Berlin Heidelberg: Springer-Verlag, 2011. ISBN: 978-3-642-17495-7. URL: https://www.springer.com/gp/book/9783642174957 (visited on 07/24/2019).

[45] P. Sahoo. *Probability and mathematical statistics*. Louisville, 2013.

[46] C. Shepard, H. Yu, N. Anand, E. Li, T. Marzetta, R. Yang and L. Zhong. Argos: practical many-antenna base stations. en. *Proceedings of the 18th annual international conference on Mobile computing and networking - Mobicom '12*. Istanbul, Turkey: ACM Press, 2012, 53. ISBN: 978-1-4503-1159-5. DOI: 10.1145/2348543.2348553. URL: http://dl.acm.org/citation.cfm?doid=2348543.2348553 (visited on 03/20/2019).

[47] L. Smaini. *RF Analog Impairments Modeling for Communication Systems Simulation: Application to OFDM-based Transceivers*. English. 1 edition. Hoboken, New Jersey: Wiley, Oct. 2012. ISBN: 978-1-119-99907-2.

[48] J. V. Stone. Information Theory: A Tutorial Introduction. (), 24.

[49] L. M. Surhone, M. T. Timpledon and S. F. Marseken. *Wishart Distribution: Statistics, Chi-Square Distribution, Gamma Distribution, John Wishart (statistician), Probability Distribution, Matrix (mathematics), Random Variable*. en. Google-Books-ID: W_RERAAACAAJ. Betascript Publishing, June 2010. ISBN: 978-613-0-36231-7.

[50] T. Svantesson. Modeling and estimation of mutual coupling in a uniform linear array of dipoles. *1999 IEEE International Conference on Acoustics, Speech, and Signal Processing. Proceedings. ICASSP99 (Cat. No.99CH36258)*. Vol. 5. Mar. 1999, 2961–2964 vol.5. DOI: 10.1109/ICASSP.1999.761384.

[51] R. Vaughan and J. B. B. Andersen. *Channels, Propagation and Antennas for Mobile Communications*. English. London: The Institution of Engineering and Technology, Feb. 2003. ISBN: 978-0-85296-084-4.

[52] J. Vieira, F. Rusek and F. Tufvesson. Reciprocity calibration methods for massive MIMO based on antenna coupling. *2014 IEEE Global Communications Conference*. Dec. 2014, 3708–3712. DOI: 10.1109/GLOCOM.2014.7037384.

[53] H. Wei, D. Wang and X. You. Reciprocity of mutual coupling for TDD massive MIMO systems. *2015 International Conference on Wireless Communications Signal Processing (WCSP)*. Oct. 2015, 1–5. DOI: 10.1109/WCSP.2015.7340979.

[54] H. Wei, D. Wang, H. Zhu, J. Wang, S. Sun and X. You. Mutual Coupling Calibration for Multiuser Massive MIMO Systems. *IEEE Transactions on Wireless Communications* 15.1 (Jan. 2016), 606–619. ISSN: 1536-1276. DOI: 10.1109/TWC.2015.2476467.

[55] H. Yang and T. L. Marzetta. Performance of Conjugate and Zero-Forcing Beamforming in Large-Scale Antenna Systems. *IEEE Journal on Selected Areas in Communications* 31.2 (Feb. 2013), 172–179. ISSN: 0733-8716. DOI: 10.1109/JSAC.2013.130206.

[56] C. Zhang, J. Ni, Y. Han and G. Du. Performance analysis of antenna array calibration and its impact on beamforming: A survey. *2010 5th International ICST Conference on Communications and Networking in China*. Aug. 2010, 1–5.

[57] J. Zhang, Y. Wei, E. Björnson, Y. Han and S. Jin. Performance Analysis and Power Control of Cell-Free Massive MIMO Systems With Hardware Impairments. *IEEE Access* 6 (2018), 55302–55314. ISSN: 2169-3536. DOI: 10.1109/ACCESS.2018.2872715.

[58] Y. Zou, O. Raeesi, R. Wichman, A. Tolli and M. Valkama. Analysis of Channel Non-Reciprocity Due to Transceiver and Antenna Coupling Mismatches in TDD Precoded Multi-User MIMO-OFDM Downlink. *2014 IEEE 80th Vehicular Technology Conference (VTC2014-Fall)*. Sept. 2014, 1–7. DOI: 10.1109/VTCFall.2014.6965875.

A ETHICAL, ECONOMIC, SOCIAL AND ENVIRONMENTAL ASPECTS

A.1 Introduction

The so-called fifth-generation (5G) is raising high expectations in many different fields, as it promises substantially increasing spectral efficiency, energy efficiency and peak data rates, among others, compared to previous generations. Achieving these goals is a major challenge and massive multiple-input multiple-output (MIMO) is the most promising key technology to improve system performance in such away.

This technology consists of deploying a large number of antennas at the base stations, in the order of hundreds of antenna elements, compared to a small number of users being served. This work studies one of the possible limitations that can be found in the implementation of this new technology, massive MIMO, and also focuses on promising new architecture.

A.2 Description of relevant impacts

In this appendix, we analyse how the context of this project can impact on aspects as diverse as economy, environment or ethics and professionalism.

We consider them to be the most important impacts to take into account because 5G and massive MIMO promise to reduce consumption cost, improve energy efficiency and change the paradigm of many jobs. We present a detailed analysis below.

- **Environmental impact:** More efficient architecture or techniques can reduce power consumption, and better efficiency affects network operators that reduce operating costs. Additionally, cutting down on power consumption implies a lower impact on the environment. This impact affects the whole society, the environment and the network operator.
- **Ethics and professionalism:** Requirements, which until nowadays could not be met, allow to create a new paradigm in many risky professions. Reducing risks facilitates compliance with occupational safety laws, and therefore, benefiting both employees and employers.

A.3 Detailed analysis of the main impacts

The promised improvements by these new technologies do not consist solely in enhance performance, but also increase efficiency. This means that resources are used more efficiently than before, i.e. to provide the same quality of service the needed amount of energy is drastically reduced.

The environmental impact is evident, an energy efficiency enhancement translates into a lower carbon footprint of the infrastructure, thereby achieving a considerable reduction in the environmental impact due to the operation of the base stations. Improving efficiency is not only relevant in social aspects, but it also has a strong economic impact on the company that operates the infrastructure. Reducing energy consumption reduces electricity cost and also reduces the cost of cooling base stations, both imply cutting operating expenses.

Furthermore, this technology can be the key to allow applications that have not even been conceived yet or that for requirements the reliability or low latency have not been able to be implemented until now. By setting an example, if high transmission rates and ultra-low latency are achieved it would be possible to control dangerous machines in real-time from the safety of a control station, this would mean eliminating risks in many dangerous jobs; hence, improving working conditions of countless jobs. This could be extremely important in terms of ethics and professional responsibility.

A.4 Conclusions

This work does not have a direct impact on the social or economic spheres, but it is technical research and development what allows all these promising goals to be carried out. Scientific works are key enablers of the next wireless generations that will critically impact on many different aspects of our lives.

We sum up the previously considered implications of these new technologies as follows

- Reducing the **carbon footprint** of network infrastructures;
- Improving **working conditions** by avoiding risk scenarios;
- Cutting **operating expenses** of network infrastructures;

Although this work and many others do not study the mobile networks as a whole, without different kind of works complementing each other, mobile networks would not be a reality. Hence to a certain extent, this work and similar ones are involved in the previously mentioned aspects.

B ECONOMIC BUDGET

Labour cost (Direct cost)		**Amount hours**	**Price/hour**	**Total**
		810	15 €	**12150 €**
Cost of material resources (Direct cost)	**Price**	**Months of use**	**Depreciation (years)**	**Total**
Personal computer	1500 €	6	5	**150 €**

Expendable material		
Printing		**100 €**
Book binding		**60 €**
Subtotal		12460 €
Taxes	21 %	2616.6 €
Total Budget		**15076.6 €**

Table B.1. *Economic budget*